Bi-monthly • Jan - Feb • 2014

ISSN: 0976-2108

BARC
NEWSLETTER

भाभा परमाणु अनुसंधान केंद्र
BHABHA ATOMIC RESEARCH CENTRE

IN THIS ISSUE

- Modeling The Flow Characteristics During Start-Up of Natural Circulation Systems from Rest State
- Time Frequency based Algorithm for Online Detection of Thermal Hydraulic Instabilities in AHWR
- Under Sodium Ultrasonic Imaging System for PFBRV
- Applications of Digital Reactivity Meter based on Kalman Filtering Technique in Indian Nuclear Reactors
- Measurement of Internal Diameter of Pressure Tubes in Pressurized Heavy Water Reactors using Ultrasonics

In the forthcoming Issue

1. Isotope techniques for water resources development and management
   Archana S. Deodhar et al. IARD

2. Total reflection x-ray fluorescence spectrometry for characterization of nuclear materials
   N. L. Mishra et al., FCD

3. Cobalt shapes for radio-isotope application from an indigenous source
   B. Paul et al., MPD

4. Compositional characterization of materials using neutron and proton based nuclear analytical methods
   R. Acharya et al. RCD

5. Transgenic approaches for development of disease resistance in banana
   Ganapathi, T.R., NABTD

CONTENTS

Editorial Note ii

Brief Communication

- Development of Suspendable Servo Manipulator for Activity Reduction in Vitrification Cell - WIP, Trombay iii

Book Reviews

- Functional Materials: Preparation, Processing and Applications iv
  (Eds. S. Banerjee and A.K. Tyagi)
- Thoria-based Nuclear Fuels: Thermophysical and Thermodynamic Properties, Fabrication, Reprocessing, and Waste Management. iv
  (Eds. Dr. D. Das, Dr. S.R. Bharadwaj)

Research Articles

- Modeling The Flow Characteristics During Start-Up of Natural Circulation Systems from Rest State 1
  Naveen Kumar, A.K. Nayak, P.K. Vijayan and K.K. Vaze
- Time Frequency based Algorithm for Online Detection of Thermal Hydraulic Instabilities in AHWR 12
  Ch Santosh Subudhi, S.R. Shimjith and A.P. Tiwari

Technology Development Articles

- Under Sodium Ultrasonic Imaging System for PFBR 18
  H. Patankar, S.K. Lalwani, A.A. Agashe, G.D. Randale, R. Chaurasia, P. Jyothi, R.K. Jain, S. Srivastava, T.S. Ananthakrishnan and C.K. Pithawa
- Applications of Digital Reactivity Meter based on Kalman Filtering Technique in Indian Nuclear Reactors 25
  R.K. Patil and S.R. Shimjith
- Measurement of Internal Diameter of Pressure Tubes in Pressurized Heavy Water Reactors using Ultrasonics 31
  Manojit Bandyopadhyay, Amit K Haruray, A.M. Kadu, Gurpartap Singh, H.M. Bapat, M. Padmanabhan, R.K. Puri and D.N. Badodkar

News & Events

- National Symposium on Very High Energy Gamma – Ray Astronomy (NSGRA-2013): a report 38
- Report of Conference on Neutron Scattering (CNS-2014) 39
- Report on National Symposium on Nuclear Instrumentation – 2013 (NSNI-2013) 40
- Resistive Plate Chambers installed for the new layer added to CMS muon system at CERN 41
- The Nineteenth National Symposium & Workshop on Thermal Analysis (THERMANS-2013) 43

BARC Scientists Honoured 44

From the Editor's Desk

The first issue of 2014 is now with you. The cover page has been changed to present a better look. We would like to sincerely thank all the scientists and engineers who have contributed their articles to BARCNL during 2013. Over the years BARCNL has become an important medium to express our major achievements and we are happy that the readership has increased both in India and abroad. This year due to unavoidable circumstances, there was a delay in the publication of the issue and we sincerely regret this delay.

This issue carries Five articles and a Brief Communication. One of the articles addresses the important issue of nuclear safety in advanced reactor designs; the reliability assessment of natural circulation systems. Another article deals with the design and development of a novel Non Contact Ultrasonic Inspection System (NCUIS) to check the functionality of the high-temperature and contaminated transducers of the Under Sodium UltraSonic Scanner (USUSS), for the Prototype Fast Breeder Reactor. The air-coupled ultrasonic technique was used to develop the system.

Recently, BARC Scientists published two books: One on Functional Materials and the other on Thoria-based Nuclear Fuels. The first one was published by Elsevier and the other by Springer-Verlag. This issue carries a brief review about the two published books which would be of interest to our colleagues.

Dr. K. Bhanumurthy
On behalf of the Editorial Committee

Development of Suspendable Servo Manipulator for Activity Reduction in Vitrification Cell - WIP, Trombay

Design, Manufacturing & Automation Group
and
Nuclear Recycle Group

Induction heated metallic melter has been deployed at Waste Immobilisation Plant (WIP), Trombay, for vitrification of high level radioactive waste. Vitirified product from melters is poured into stainless steel canisters for interim storage and its subsequent disposal in geological disposal facilities. During the completion of pouring of molten vitreous mass, a few glass-threads get formed at the bottom part of process pot due to physic-chemical properties of glass. These threads invariably get collected in the canister itself but on a few occasions, it falls on the turn table during handling of canisters. These threads are generally very small in sizes with an average diameter of 4 mm and length of 50 mm. Existing remote handling tools are used for lifting these glass threads. However, a few glass threads remain inaccessible, because of limited reach of the remote handling gadgets. Suspended Servo Manipulator (SSM) developed by Division of Remote Handling and Robotics (DRHR), BARC was deployed after extensive mock trials to lift remaining glass threads fallen at inaccessible areas during recently completed vitrification campaign. With the joint effort of Waste Management Division (WMD, NRG) and DRHR, campaign of picking up of about 30 number of glass threads of smaller sizes were successfully completed resulting in a substantial dose reduction within the hot-cell.

The suspendable Servo Manipulator [Fig.1] is a novel design consisting of a slave and a master arm, connected to a controller through electric cables. The slave arm is suspended onto the crane hook and taken to the site remotely. It has five degrees of freedom and gripper, all controlled by electric motors. The major joints of the slave arm are mechanically balanced to reduce the swing of the arm, during motion. The master arm is small and kinematically similar to that of the slave arm. Remote operations are viewed through in-cell cameras and additional cameras mounted on the slave arm [Fig. 2 & 3].

Fig.1: Suspendable Servo Manipulator (SSM)

Fig.2: Master Arm of SSM in the Control Room

Fig.3: Active Glass Thread Picked-Up by SSM

Functional Materials: Preparation, Processing and Applications

(Eds. S. Banerjee and A. K. Tyagi)
Elsevier Insights (ISBN: 978-0-12-385142-0)

Recently a book titled "Functional Materials: Preparation, Processing and Applications (Eds. S. Banerjee and A. K. Tyagi)" was published by Elsevier Insights. The major highlight of this book is that all the chapters have been contributed by scientists from BARC. Thus a wide spectrum of research on functional materials, being carried out at BARC, could be showcased.

The functional materials are categorized solely based on their functional properties and their prospective applications. They have assumed very prominent position in several high tech areas. The book encompasses a wide panorama of functional materials such as super-strong materials, soft materials, magnetic materials, multi-ferroics, spintronics, carbon based materials, conducting polymers, optical materials, glasses, nuclear fuels, corrosion resistant materials, materials for hydrogen production and storage, and electro-ceramics. Each chapter broadly discusses physical basis of the functionality, materials synthesis and processing, characterization, properties and applications. We hope that this book will be of use to both new and experienced researchers in the field.

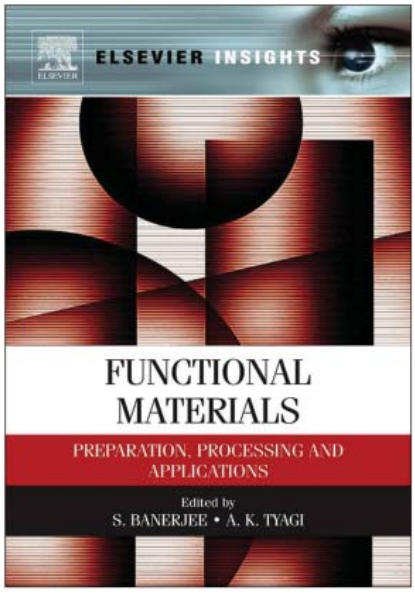

Thoria-based Nuclear Fuels

Thermophysical and Thermodynamic Properties, Fabrication, Reprocessing, and Waste Management.

Dr. D. Das, Dr. S. R. Bharadwaj (Eds.)
Chemistry Division

This book presents the state of the art on thermophysical and thermochemical properties, fabrication methodologies, irradiation behaviours, fuel reprocessing procedures, and aspects of waste management for oxide fuels in general and for thoria-based fuels in particular. The book covers all the essential features involved in the development of and working with nuclear technology. With the help of key databases, many of which were created by the authors, information is presented in the form of tables, figures, schematic diagrams and flow sheets, and photographs. This information will be useful for scientists and engineers working in the nuclear field, particularly for design and simulation, and for establishing the technology. One special feature is the inclusion of the latest information on thoria-based fuels, especially on the use of thorium in power generation, as it has less proliferation potential for nuclear weapons. Given its natural abundance, thorium offers a future alternative to uranium fuels in nuclear technology. In closing, the latest information on conventional uranium and plutonium fuels is also provided.

This book is published by Springer-Verlag, London (2013), 418 Pages and 173 Illustrations.

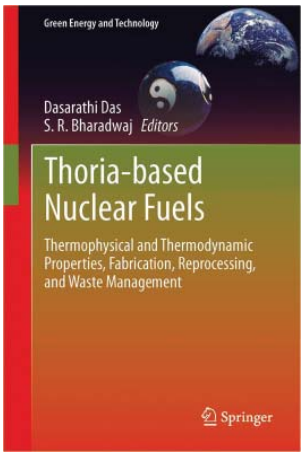

Modeling The Flow Characteristics During Start-Up of Natural Circulation Systems from Rest State

Naveen Kumar, A.K. Nayak, P.K. Vijayan and K.K. Vaze
Reactor Engineering Division

Abstract

Most of the advanced reactor designs propose to use natural circulation for core heat removal either during normal operational states and/or during off-normal operational states because of simplicity and higher reliability of natural circulation. However, these systems do have their own set of challenges with respect to assessment of their reliability. Simulation of start-up from rest and performance evaluation using conventional models are the key issues in assessing their reliability. In view of their wide importance to nuclear safety, the performance of these systems during start-up from rest is addressed in the present study.

Introduction

Passivity and simplicity are the hallmark of any good engineering design. These features are perhaps nowhere more desirable than in nuclear systems where safety of both the plant and the public at large is of prime concern. Passivity, the ability to operate without reliance on any external power source, enhances the safety. Simplicity, avoidance of complex piping and logics, makes the system operation and maintenance considerably easy. A natural circulation system has both passivity and simplicity inbuilt in it. It is because of these desirable features that these systems find wide application in many industrial systems like nuclear power plants, solar heating and cooling systems, geothermal systems, electrical machine rotor cooling, turbine blade cooling, electronic device cooling and process industry. Many of the next generation nuclear power plants propose to use natural circulation as the heat removal mode either during normal operational states and/or during off-normal operational states. Indian Advanced Heavy Water Reactor (AHWR) and Prototype Fast Breeder Reactor (PFBR), Westinghouse's AP-1000, General Electric's Economic Simplified Boiling Water Reactor (ESBWR), Russian VVER-1000 and Argentina's CAREM, are just to name a few. Despite the philosophy of defense-in-depth, electromechanical active components and/or human operations are likely to fail as exemplified by the accidents at Three Mile Island-2, Chernobyl-4 and Fukushima.

Decay heat, if not removed, can result in overheating and damage to the fuel. Hence, most of the advanced reactor designs propose to use natural circulation for decay heat removal during the off normal conditions.Like any other system, the natural circulation systems also do have their own set of challenges. Though passive systems are highly reliable, in reality there exists a non-zero probability that these system fail to perform the intended function. Therefore, a reliable prediction of their performance is of utmost importance for their successful deployment. Natural circulation systems have low driving force and need to be started from the state of rest. Start-up from rest is one of the key issues in assessing the reliability of these systems. There is always a finite time lag before these systems attain their optimum/intended performance level. Further, the models applicable under low flow conditions can be quite different from those applicable under high flow conditions. For example, under low flow conditions, the flow

is essentially multi-dimensional and hence classical 1-D may not predict their behaviour with reasonable satisfaction. Also the performance of these systems is strongly dependent on the operating conditions and system geometry. Owing to the very dependence of system flow rate (and hence heat removal capability) on operating conditions, any change in operating conditions may have a bearing on their overall performance. This article addresses some of these issues.

Model for start-up from rest

During the start-up of a natural circulation system, the flow is essentially single-phase and hence, single-phase natural circulation is important to all the natural circulation systems. Unlike forced circulation systems where flow gets established as soon as the fluid moving device is put on, in a natural circulation system, the flow is generated by the temperature difference between the source and the sink. In a forced circulation system, the flow through the system is established first by putting on the fluid moving machinery. This is followed by activation of heater power, e.g. chain reaction in a nuclear power plant and electrical heating in experimental facilities. However, in a natural circulation system, the sequence is reverse. Since both source and the sink are at the same temperature to start with, initially there is no flow through the system. Hence, the heater power needs to be raised to some positive non-zero value before flow gets established through the system. The problem is further complicated by the orientation of the heat source and sink. Heat source can be vertical as in AHWR or ESBWR or horizontal as in PHWRs. Similarly sink can also be horizontal as in VVERs or vertical as in PHWRs.While in systems having vertical heater the onset of bulk fluid circulation is almost immediate for moderate heater powers, in loops having heaters in horizontal leg, the bulk circulation is always preceded by some quiescent period. In systems having horizontal heaters, the flow does not take place till the hot fluid reaches the vertical leg. This has a bearing on the peak heater element temperature and hence on the integrity of the fuel or heating element. Present 1-D models, which continue to be the workhorse for reactor thermal hydraulics and safety analysis, fail to predict the start-up of natural circulation systems having heat source in horizontal leg. Under low or no flow (circulation) conditions, the heat is transferred from the heated sections to unheated sections by natural convection. These currents were referred as secondary currents by Bau and Torrence[1]. These currents are essentially multi-dimensional in nature. They are relevant not only during start-up but also during the transients whenever low flow conditions are encountered. It is because of the inability of present 1-D models to account for these local convection currents that these models fail to predict the start-up of these systems from rest reliably.Numerical simulations carried out using system codes like ATHLET [2], RELAP5 [3] and CATHARE [4] show that start-up of these loops cannot be simulated using classical 1-D models. Fichera and Pagano [5] accounted for these currents by taking an arbitrarily high value of molecular thermal diffusivity in their numerical simulations.In the present study, a pseudo-conductivity model has been presented to account for these secondary convection currents. The proposed model is based on scale analysis. It has been validated against CFD simulations and incorporated in a 1-D model. The results of numerical simulations for start-up of single-phase natural circulation systems having different heater and cooler configurations are presented.

Governing Equations

The mathematical model is based on the following simplifying assumptions:

(a) The flow can be represented by a 1-D description that does not take into account for radial variation of the fluid properties.

(b) Heat generation in the fluid due to frictional dissipation and macroscopic terms, i.e. kinetic and potential energy are neglected in the energy equation.

(c) Each fluid element is in thermal contact with a heat structure and a convective heat transfer boundary condition can be assigned to the outside surface of the structure, specifying the outer fluid temperature and the outer heat transfer coefficient.

(d) For a nearly incompressible fluid, natural convection consists of two equal and opposite streams moving between cold and warm sections. There is zero net mass transfer between the two sections and a net energy exchange. The energy change can be accounted in the area averaged energy balance equation.

With the above assumptions the governing mass, momentum and energy balance equations for flow through a channel are written as:

$$\frac{\partial \rho}{\partial t} + \frac{1}{A}\frac{\partial W}{\partial s} = 0 \tag{1}$$

$$\frac{1}{A}\frac{\partial W}{\partial t} + \frac{1}{A}\frac{\partial}{\partial s}\left(\frac{W^2}{\rho A}\right) = -\frac{f}{D}\frac{W^2}{2\rho_l A^2} - \frac{\partial p}{\partial s} - \rho g \sin\theta \tag{2}$$

$$\frac{\partial}{\partial t}(\rho h) + \frac{1}{A}\frac{\partial}{\partial s}(Wh) - \frac{\partial p}{\partial t} = \frac{\lambda_l P\left(T_w - T_f\right)}{A} + \frac{1}{A}\frac{\partial}{\partial s}\left(AK_{eff}\frac{\partial T}{\partial s}\right) \tag{3}$$

$$\rho = \rho\left(p, h\right) \tag{4}$$

For the solution of governing equations, these are discretized using staggered mesh. The computational domain is divided into non-overlapping rigid control volumes, called cells. The field variables, h, p and ρ are defined at the cell centers, while the fluid mass velocity, W is defined at cell interfaces also called junctions. The discretized equations are presented in Naveen Kumar [6].

Evaluation of K_{eff} – Pseudo-conductivity Model

K_{eff} in equation (3), known as effective conductivity, is evaluated using the pseudo-conductivity model described here. In a natural circulation loop having heater in the horizontal section, the fluid is motionless and is at same temperature to start with. When the heater is switched on and power is made greater than zero, the fluid in the heated portion starts getting heated up. This hot fluid spreads sideways into the unheated section by local natural convection. For an incompressible fluid, these currents lead to net energy transfer from the heated section to unheated section without any net mass transfer across the pipe cross section. Hence, these currents can be thought like pseudo-conduction. During the start-up of natural circulation loops having horizontal heater, the natural convection currents are confined to the horizontal pipe section only and the fluid behavior is similar to that in a slender horizontal cavity closed at both the ends. During this phase, the area averaged net flow at any cross section remains zero and there is a net heat transfer at the interface between hot and cold sections. The rate of heat transfer across any cross-section depends upon the net forward or backward (both are equal in magnitude for an incompressible fluid) mass flow rate at that cross section and the difference in temperatures of two stream. Naveen Kumar et al. [6-7] studied the natural convection in slender pipes closed at both the ends. In this study it was shown that the magnitude of cross section area averaged forward or backward velocity (backward and forward currents are equal in magnitude but opposite in direction) for horizontal and vertical pipes is given by the following expression:

$$u_{nc,j} = \begin{cases} 0.99\left(\alpha/D\right)\left(Ra_D\right)^{1/2} & for\ horizontal\ \ cells \\ 0.0018\left(\alpha/D\right)Ra_D & for\ vertical\ \ cells \end{cases} \tag{5}$$

It is worth noting here that the velocities given by equation (5) are area averaged forward or backward (in case of a vertical cavity, it is upward

or downward) velocities at any cross section under steady state conditions. However, during natural convection, the forward current is expected to be confined to half of the pipe cross section and the backward current is expected to be confined to the other half of pipe cross section. Therefore, the convection currents will move twice as fast as that given by equation (5). For a loop having horizontal heater, the heat transfer by natural convection can exist in horizontal section whenever natural circulation flow is small e.g., during start-up of such systems from no flow condition. However, for a vertical pipe section, this can happen whenever a hot fluid pocket lies below a cold fluid pocket e.g., during the transient the hot pocket may be lying below the cold pocket, and the hot and cold fluid packets may be distributed in two legs such that the loop flow is near zero. These conditions are expected during the transient unstable flow conditions and have been observed experimentally by Vijayan et al. [8]. Naveen Kumar [6] showed that the net energy exchange per unit area by these local convection currents is given by the following expression:

$$q''_{nc} = \begin{cases} 0.99\left(k_f/D\right)Ra_D{}^{1/2}\Delta T & for\ horizontal\ \ cells \\ 1.8x10^{-3}\left(k_f/D\right)Ra_D\Delta T & for\ vertical\ \ cells \end{cases} \quad (6)$$

Thus in the absence of any bulk fluid motion, the steady state heat transfer between the cold and hot sections, maintained at a temperature difference of ΔT, consists of two components: conduction and natural convection. Mathematically, it is written as

$$q'' = q''_{cond} + q''_{nc} = -k_f\left(\Delta T/\Delta s\right) + h_{nc}\Delta T \quad (7)$$

$$\text{where } h_{nc} = \begin{cases} 0.99\left(k_f/D\right)Ra_D{}^{1/2} & Horizontal\ \ pipe \\ 0.0018\left(k_f/D\right)Ra_D & Vertical\ \ pipe \end{cases} \quad (8)$$

For ease of interpretation, equation (7) is written as

$$q'' = -K_{eff}\left(\Delta T/\Delta s\right) \quad (9)$$

$$\text{where } K_{eff} = k_f + h_{nc}\Delta s \quad (10)$$

K_{eff} is the effective thermal conductivity which takes into account the heat transfer by both conduction and natural convection. The first term in equation (10) is the molecular conductivity of the fluid and accounts for axial heat transfer by conduction in the fluid. The second term accounts for heat transfer by local natural convection between two volumes (pipe sections) filled with fluids having different temperatures. However, unlike the fluid thermal conductivity, which is a property of fluid, the magnitude of pseudo-conductivity depends on the temperature difference between the two fluid volumes. Thus, the effect of natural convection can be accounted in 1-D model by using an effective thermal conductivity as given by equation (10). Advantage of this approach is that it can easily be incorporated in the conventional 1-D models without any major modifications. Also, this approach has the advantage of being computationally cost effective.

Local convection is the dominant mechanism of heat transfer till the natural circulation flow is zero. With the onset of bulk flow (circulation), the fluid starts moving either in clockwise or anti-clockwise direction throughout the loop. The fluid flow is now just like forced convection through a pipe. With the onset of bulk fluid motion, these currents start diminishing and eventually get suppressed completely when loop flow rate increases sufficiently. Hence, the heat transport mechanism in a natural circulation loop passes from the phases of local natural convection to mixed convection to natural circulation. A proper simulation of loop dynamics requires not only proper models for each regime but also the knowledge of criterion

for transition from one regime to another. Naveen Kumar et al. [7] presented the following criterion for transition between natural convection and natural circulation:

$$h_{nc} = \begin{cases} \left(1-\left|\bar{u}_j/u_{nc,j}\right|\right)h_{nc} & if \quad \left|\bar{u}_j\right| \le \left|u_{nc,j}\right| \\ 0 \quad if \quad \left|\bar{u}_j\right| > \left|u_{nc,j}\right| \end{cases} \quad (11)$$

The above criterion is based on the relative strength of natural convection and natural circulation currents. The relative strength of natural convection to natural circulation is given by the ratio of the characteristic natural convection velocity, $u_{nc,j}$ and the natural circulation velocity, $\bar{u}_j$. It can be seen from equation (11) that pure natural convection is the heat transfer mode when natural circulation ($\bar{u}_j$) velocity is zero and natural circulation is the heat transfer mode when natural circulation velocity ($\bar{u}_j$) is greater than natural convection velocity ($u_{nc,j}$). The mixed convection regime lies between these two regimes. This regime is taken into account in the above criterion by introducing the factor $\left(1-\left|\bar{u}_j/u_{nc,j}\right|\right)$ in equation (11). The reasons for adopting such a criterion are explained below. The natural convection currents are essentially multi-dimensional in nature even in small diameter pipes and develop fully only in the absence of forced convection (global natural circulation) currents. However, forced convection currents are strongly directional in nature and involve either movement of fluid from the cold section to the hot section or from the hot section to the cold section. There is net flow across the interface. As one moves away from natural convection regime to mixed convection regime, these natural circulation (bulk loop flow) currents start interfering with natural convection currents. This impedes the development of natural convection currents thereby hindering the energy transfer by natural convection across the interface. This has been taken into account in equation (11) by introducing the factor $\left(1-\left|\bar{u}_j/u_{nc,j}\right|\right)$. The criterion given by equation (11) blends the switching from natural convection to natural circulation in a continuous fashion. The pseudo-conductivity model has been validated by comparing the model predictions with CFD simulations for circular horizontal and vertical cavities closed at both the ends [6-7].

Role of constitutive laws for wall friction

The inability of conventional friction factor correlations applicable for forced circulation under adiabatic conditions to predict pressure drop under diabatic conditions was recognized long back by Deissler[9]. Ambrosini and Ferreri[10] showed that accurate and reliable prediction of loop stability and transient behaviour is strongly dependent on the choice of friction factor. Naveen Kumar [6] proposed the following correlation for friction factor for flow through horizontal pipes:

$$f_F = f_L\left[1+\left(f_{Tt}/f_L\right)^{6.4}\right]^{1/6.4} \quad (12)$$

where

$$f_{Tt} = f_T\left[1+\left(f_t/f_T\right)^{-2}\right]^{-\frac{1}{2}} \quad (13)$$

$$f_L = \left(16/\mathrm{Re}\right)\left\{1+\left(1.56Ra_f^{\,0.15}\right)^{15}\right\}^{1/15} \quad (14)$$

$$f_T = 0.0791\mathrm{Re}^{-0.25}\left(\mu/\mu_w\right)^{-0.2} \quad (15)$$

$$f_t = 0.03862\left(\mathrm{Re}/2000\right)^6 \quad (16)$$

The correlation given by equation (12) was derived from steady state experimental data by Naveen Kumar [6]. A comparison of the proposed correlation with conventional forced convection laws is shown in Fig. 1. It is seen from the Fig 1 that the conventional forced friction factor laws overpredict the loop mass flow rate (higher Ress for a given Grm/NG). A similar type of correlation showing dependence on local Rayleigh number is expected for vertical pipe sections also. However, in the absence of any such correlation, the wall friction in vertical sections has been evaluated using conventional forced friction correlation. To sum up,

the model uses the following correlation for wall friction:

$$f_F = \begin{cases} Eq.(12) & Horizontal \quad pipes \\ \left[16/\mathrm{Re},\ 0.079/\mathrm{Re}^{0.25}\right] & Vertical \quad pipes \end{cases} \quad (17)$$

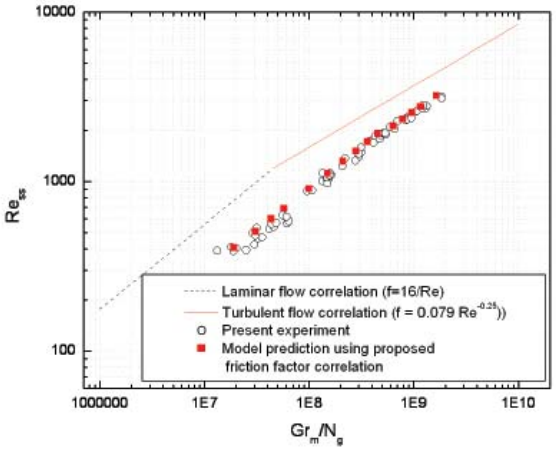

Fig. 1: Comparison of model predictions made using proposed friction factor correlation with experimental data.

Flow characteristics of single-phase natural circulation during start-up

The model developed has been applied to simulate the start-up of natural circulation loop shown in Fig. 2. The loop consists of a uniform diameter rectangular natural circulation loop. The details of the experimental setup are given in Vijayan et al. [4]. It has two heaters and two coolers. One of the heaters is at lowest elevation and the other one is in vertical section. Similarly, one of the coolers is placed in the horizontal section at the uppermost elevation and the other cooler is placed in vertical pipe section. It is possible to run the loop in any of the following four configurations:

(a) Horizontal Heater and Horizontal Cooler (HHHC)
(b) Horizontal Heater and Vertical Cooler (HHVC)
(c) Vertical Heater and Horizontal Cooler (VHHC)
(d) Vertical Heater and Vertical Cooler (VHVC)

The addressed loop with different combinations of heaters and coolers can be considered as representative of different natural circulation systems encountered in the industry.

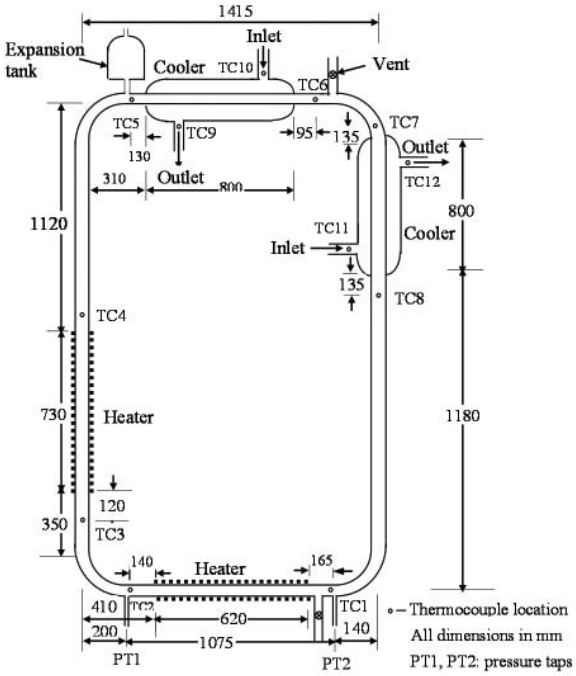

Fig. 2: Schematic of natural circulation loop [8]

Studies for horizontal heater configuration

The model developed has been applied for the simulation of loop transient behavior from state of rest conditions. The initial fluid temperature is assumed to be same throughout the loop and the expansion tank. In the test facility, the heater is located symmetrical with respect to loop centre line. In such a facility, there is equal probability of flow getting initiated in either direction. However, in numerical simulations the direction of flow initiation is dictated by the sign of initial fluid velocity which is assumed to be 1.0E-9 kg/s.

Fig. 3 shows the flow initiation transient predicted by the present model with the fluid axial heat conduction taken same as that the molecular conductivity of the fluid (h_{nc} = 0) for the HHVC

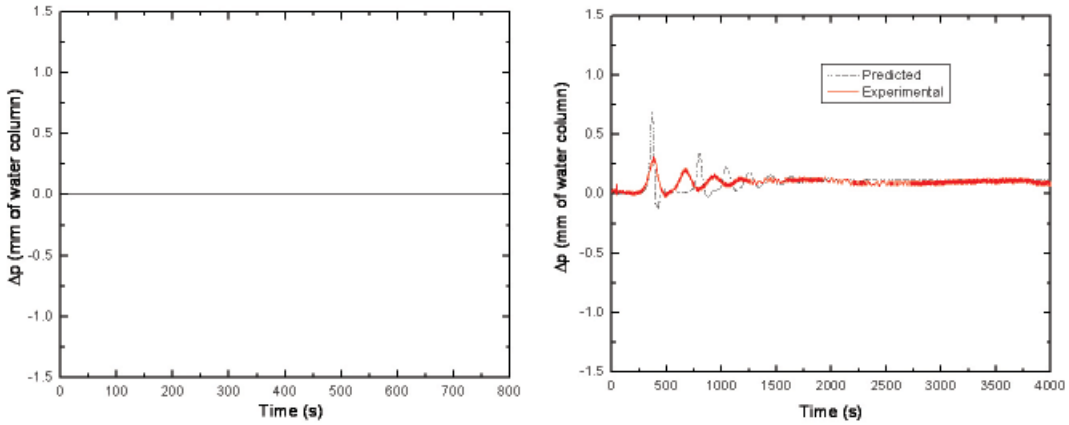

(a) hnc= 0 (b) With pseudo-conductivity model

Fig. 3: Prediction of flow initiation transient by the model developed for HHVC configuration for a heater power of 128 W.

configuration for a heater power input of 128 W. It is clear from Fig. 3(a) that the flow initiation does not take place even after a lapse of more than 800 seconds since switching on of the heater power. It was noted by Bau and Torrance [1] that mere inclusion of fluid and wall axial conduction does not help in simulating the start-up from the rest state. The same simulation is now carried out using the pseudo-conductivity model explained earlier (K_{eff}= k_f+ $h_{nc}\Delta s$). The results shown in Fig 3(b) indicates that the flow gets initiated at t = 300 seconds. This behavior has been found to be in agreement with that observed experimentally. However, the magnitude of the initial peak is greater than that observed experimentally. Also there is a mismatch in the time at which peak occurs. The mismatch between the model prediction and experimental observation can be attributed to the simplification adopted in modeling heater. The heater in the experimental test facility consists of a nichrome wire evenly wound on the glass tube. The nichrome wire makes a line contact with the glass tube and is surrounded by mineral wool from all other sides. In the heater model adopted in the numerical simulations, all the heat is assumed to be generated inside the glass tube, while in reality a portion of the heat also goes to the insulating material. This has a bearing on the flow initiation time and the magnitude of initial peak. This becomes clear from Fig 4 where the model predictions for different initial heat power inputs are compared.It is clear from Fig 4(a) that initial peak flow increases with increase in heater power input. Also the heater temperature (Fig 4(b)) increases with increase in heater power.

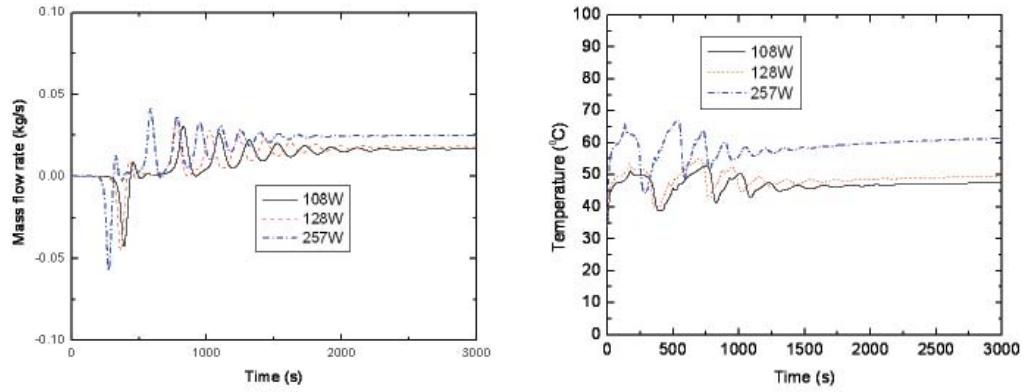

(a) Loop mass flow rate (b) Heater surface temperature

Fig. 4: Effect of heater power on flow initiation transient for HHVC configuration.

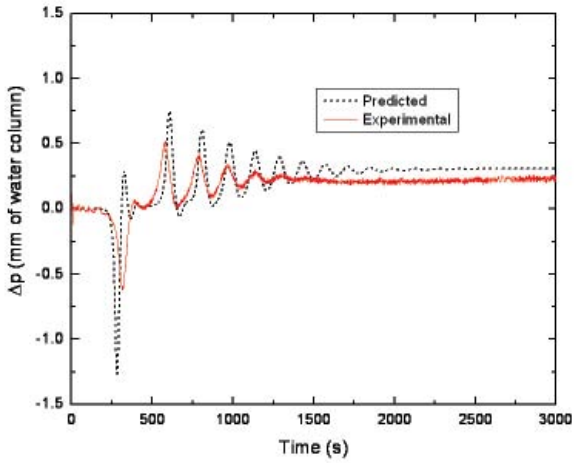

Fig. 5: Comparison of flow initiation transient predicted by the model developed with experimental behavior for HHVC configuration for a heater power of 257 W.

Vijayan et al. (2001) reported that for HHVC configuration, while there is equal probability of flow getting initiated in either clockwise or anticlockwise direction, however, only clockwise flow was found to be stable. This is shown in Fig. 5, where for a heater power input of 257 W, the flow gets initiated in anti-clockwise direction and it turns clockwise after one oscillation. A similar behavior is predicted by the model as well. Fig. 5 shows the comparison of the model predictions (made using pseudo-conductivity model) with the observed experimental behavior. The model predictions are in fair agreement with the observed experimental behavior. Fig 6 shows a comparison of model predictions with the experimental data for HHHC configuration for a heater power input of 120 W. For this configuration, both loop mass flow rate (indicated by pressure drop across heater) and fluid temperature were found to be oscillating. In fact, for this configuration, stable behaviour was observed only at powers below 55 W.

Role of expansion tank

All the closed single-phase natural circulation loops, the authors have come across are provided with an expansion tank. The tank serves the twin purposes of venting the air out during the loop filling and accommodation of the swells and shrinkages of the loop fluid during the transient. Creveling et al. [11] and Damerell and Schoenhals [12] mentioned that the interior of the loop was connected to an open reservoir; however, no details of the reservoir were reported. The loops studied by Misale et al. [4] and Fichera and Pagano [5] and Vijayan et al. [8] have expansion tank in their loops. However, only few details are available about the dimensional details of these tanks in published literature. In most works, this component is not considered important in characterizing natural circulation loop performance. In nuclear reactors also, the components like pressuriser, emergency core cooling headers etc. are also similar to expansion tank. In the present study, the expansion tank was

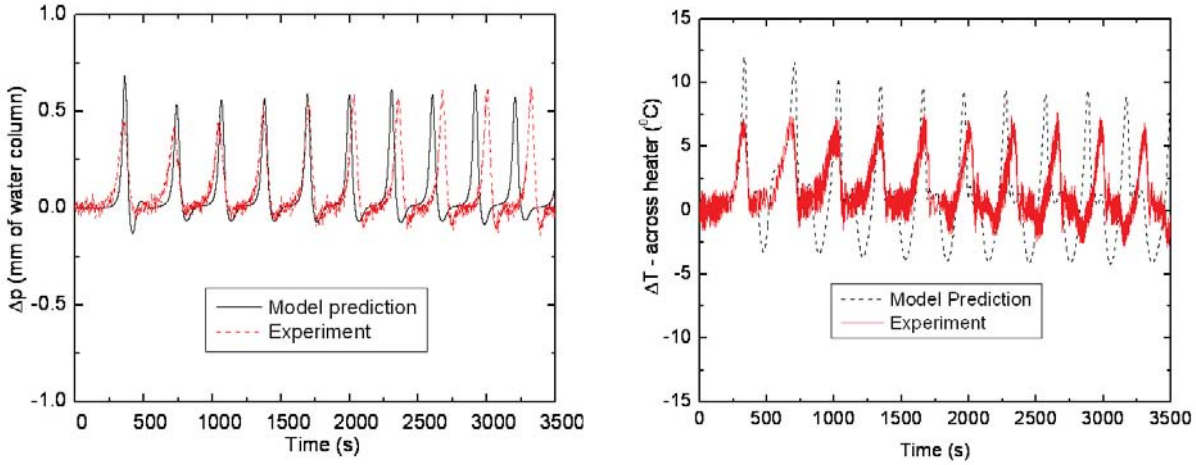

Fig. 6: Comparison of the predicted behaviour with experimental data for 120W heater power for HHHC configuration.

found to be affecting the performance of these systems.

In most of the studies, a lumped parameter model is used for modelling the expansion tank. The pressure in the tank is assumed to be constant. With these assumptions, mass, momentum and energy balance in the expansion tank take the following from:

$$\frac{dm_{TK}}{dt} = -\frac{dm_{loop}}{dt} \tag{18}$$

Neglecting frictional and acceleration losses, the momentum balance is written as

$$\left(p_{atm} - p_0^{n+1}\right) = -\rho_{TK}^n \left(L_{TK}^{n+1} + \Delta Z_L\right) g \tag{19}$$

Energy balance equation is written as

$$A_{TK} L_{TK} \frac{d}{dt}\left(\rho_{TK} h_{TK}\right) = \begin{cases} h_{m+1} \dfrac{dm_{loop}}{dt} - A_C h_{nc} \Delta T & if \dfrac{dm_{loop}}{dt} > 0 \\ -h_{TK} \dfrac{dm_{loop}}{dt} - A_C h_{nc} \Delta T & if \dfrac{dm_{loop}}{dt} < 0 \end{cases} \tag{20}$$

The first term on the right hand side of Eq. (20) represent the energy exchange with the loop because of swell/shrinkage in volume of liquid contained in the loop and the last term accounts for energy exchange between the expansion tank and the main loop by natural convection. Thus, h_{nc} in equation (20) is evaluated using the following expression:

$$h_{nc} = \begin{cases} 0.0018 \dfrac{k}{D}\left(\dfrac{g\beta D^3}{\nu\alpha}\right)\left|T_0^n - T_{TK}^n\right| & for \quad T_0^n > T_{TK}^n \\ 0 & for \quad T_0^n \le T_{TK}^n \end{cases} \tag{21}$$

D in equation (21) represents the diameter of the pipe connecting the main loop and the expansion tank and A_C is area of cross-section of the connecting pipe. In the absence of any flow through the pipe, there will be circulation of fluid between the main loop and the expansion tank if fluid temperature in the main loop is higher than that in the tank. This fluid circulation is caused by the natural convection currents and is known as natural convection heat transfer. Under pure natural convection conditions, these currents are responsible for net heat exchange between the pipe and the expansion tank. This heat exchange was found to have a bearing on loop stability behaviour by Naveen Kumar [6]. The experimental investigations in loop having geometry similar to that addressed in present study for numerical simulations (Fig. 2) showed that expansion tank temperature increases during the transient. It is worth noting that most of the numerical simulations reported in literature ignore this energy exchange between the expansion tank and the main loop by natural convection. Fig. 7 and Fig 8 show the comparison of experimentally observed behaviour with that predicted using 'Simplified Expansion Tank Model' (h_{nc} = 0) and 'Modified Expansion Tank Model' (h_{nc} given by equation (21)). It is clear from Fig 7 that simplified expansion tank model predicts unstable behaviour while modified expansion tank model predicts stable behaviour. Fig 8 shows comparison for expansion tank temperature. It is clear from Fig. 8(b) that modified expansion tank model captures the loop

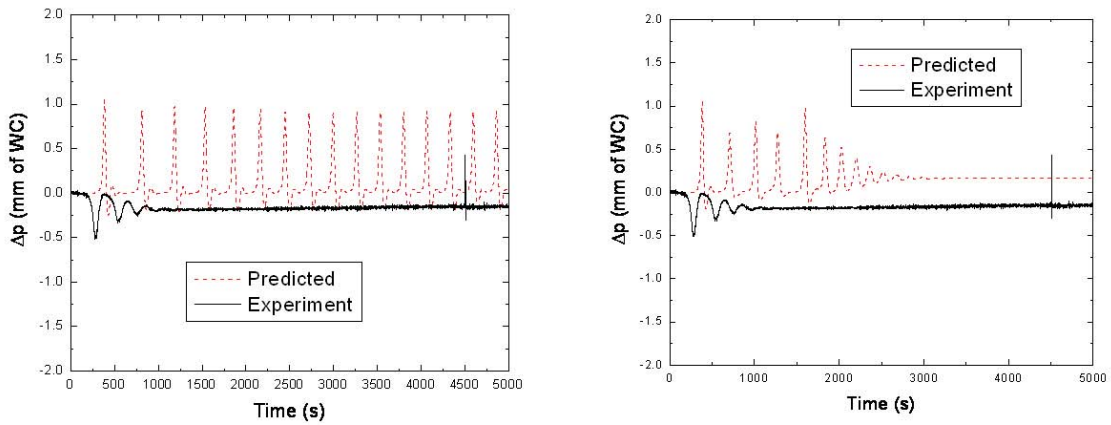

Fig. 7: Comparison of the predicted pressure drop across the heater with the experimentally observed behavior for heater power of 200W

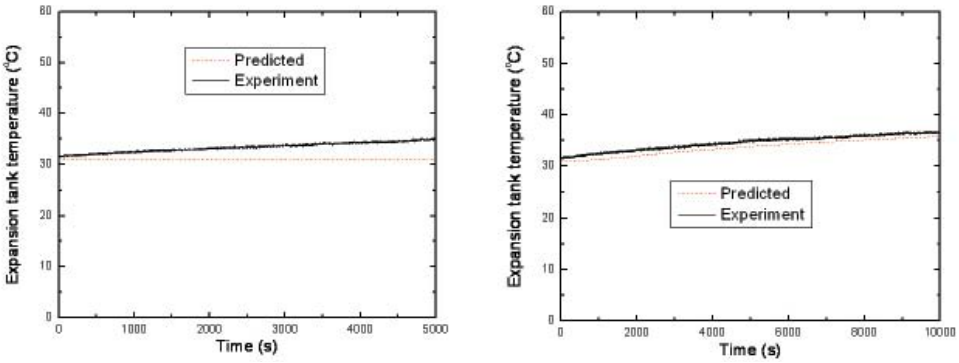

(a) Simplified expansion tank model (b) Modified expansion tank model

Fig. 8: Comparison of the predicted fluid temperature in the expansion tank with the experimentally observed behavior for heater power input of 200W

behaviour more realistically. The results presented in Fig 7 and 8 clearly show that the tanks connected to these systems may modify the operating conditions and hence the loop dynamic thermal hydraulic behaviour. In nuclear reactors, main heat transport systems have several components like pressuriser, Emergency Cooling Headers etc. connected with it. While simulating the behaviour of these systems, due consideration should be given to interaction of these systems with main loop.

Studies for vertical heater configuration

In a natural circulation loop having vertical heater, the flow initiation occurs almost immediately after the heater power is made greater than zero. This is because the buoyancy starts developing as soon as the fluid in the vertical heated section gets heated. Typical flow initiation transient predicted with model developed for VHHC configuration for a heater power input of 530W is shown in Fig. 9. The model predictions are in reasonably good agreement with the experimental behavior. However, as discussed earlier, the secondary effects (simplified heater wall dynamic model and use of wall constitutive laws derived from steady state forced convection experiments) lead to over estimation of the magnitude of the initial peak. As the hot fluid rises through the vertical pipe, it comes in contact with cold wall. When the hot fluid comes in contact with cold wall, it gets cooled, the buoyancy acts opposite to loop flow and fluid motion near the wall has a tendency to get retarded. This alters the velocity profile near the wall and may change the wall friction factor. Saylor and Joye [13] studied pressure drop in mixed convection heat transfer in vertical tubes and observed that at low Reynolds numbers and high Grashof numbers, the pressure drop for aiding flow (heating in up flow and cooling in down flow) through a vertical tube under constant temperature conditions can be orders of magnitude higher than that expected on the basis of forced flow considerations. They also observed negative pressure drop for downflow heating in mixed convection zone. Also subtle changes in model predictions made using simplified and modified expansion tank model are quite clear.

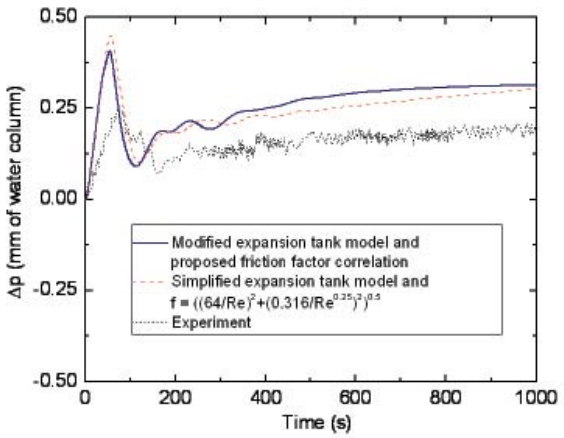

Fig. 9: Comparison of the predicted behaviour with experimental data for 530W heater power for VHHC configuration.

Conclusions

In this research, a model has been developed to predict the performance of natural circulation systems during start-up from rest. A pseudo-conductivity model has been proposed to account for multi-dimensional heat diffusion under low flow conditions. The model has been validated against the CFD simulations and successfully integrated with 1-D models which are the industry workhorse for predicting the behaviour of these systems. The model has then been used to predict the performance of a natural circulation loop having different heater and cooler orientations. The numerical predictions show that onset of flow in a NCL having horizontal heater is always preceded by some quiescent period. During this period, the heater surface temperature can rise substantially. Numerical and experimental studies show that onset of flow in a loop having vertical heater is almost immediate for moderate heater powers. The study brings out that the conventional friction factors derived from steady state forced convection experimental data are not applicable for natural circulation loops under low flow conditions. A new correlation has been proposed for wall friction for flow through horizontal tubes. In this research, the behaviour of natural circulation systems has been found to be affected by the expansion tank.

References

1. Bau, H.H., Torrance, K.E., Transient and steady behaviour of an open symmetrically heated, free convection loop, Int. J. Heat Mass Transfer 24(1981), 597-609.
2. Vijayan,P.K., Austregesilo,H., Teschendorff,V., Simulation of the unstable oscillatory behavior of single-phase natural circulation with repetitive flow reversals in a rectangular loop using the computer code ATHLET, Nucl. Eng. Des. 155(1995), 623-641.
3. Pilkhwal,D.S.,Ambrosini,W., Forgione, N., Vijayan, P.K.,Saha, D., Ferrari, J.C., Analysis of the unstable behaviour of a single phase natural circulation loop with one dimensional and computational fluid dynamics models, Ann. Nucl. Energy 34(2007), 339-355.
4. Misale, M., Frogheri,M., D'Auria,F., Fontani, E., Garcia,A., Analysis of single-phase natural circulation experiments by system codes, Int. J. Therm. Sci. 38(1999), 977-983.
5. Fichera,A., Pagano, A., Modeling and control of natural circulation loops, Int. J. Heat Mass Transfer 46(2003), 2425-2444.
6. Naveen Kumar, Investigations on start-up of natural circulation systems, Ph.D. dissertation, Indian Institute of Technology Bombay, India (2013).
7. Naveen Kumar, Doshi, J.B., Doshi, Vijayan, P.K., Investigations on the role of mixed convection and wall friction factor in single-phase natural circulation loop dynamics, Ann. Nucl. Energy 38(2011), 2247-2270.
8. Vijayan, P.K., Bhojwani, V.K., Bade, M.H., Sharma, M., Nayak, A.K., Saha, D., Sinha, R.K., Investigations on the effect of heater and cooler orientation on the steady state, transient and stability behaviour of single-phase natural circulation in a rectangular loop, Bhabha Atomic Research Centre, Report BARC/2001/E/034, 2001.
9. Deissler, R.G., Analytical investigation of fully developed laminar flow in tubes with heat transfer with fluids properties variable along the radius, NACA TN 2410, Washington DC, 1951.
10. Ambrosini,W., Ferreri, J.C., Stability analysis of single phase thermosyphon loops by finite difference numerical methods, Nucl. Eng. Des. 201(2000), 11-23.
11. Creveling, H.F., DePaz, J.F., Baladi, J.Y., Schoehnals, R.J., Stability characteristics of a single-phase free convection loop, J. Fluid Mech. 67(1975), 65-84.
12. Damerell, P.S., Schoenhals, R.J., Flow in a toroidalthermosyphon with angular displacement of heated and cooled sections, J. heat Transfer 101(1979), 672-676.
13. Saylor, P.E., Joye, D.D., Hydrostatic correction and pressure drop measurement in mixed convection heat transfer in vertical tube, Ind. Eng. Chem. Res. 30(1991), 784-788.

Time Frequency based Algorithm for Online Detection of Thermal Hydraulic Instabilities in AHWR

Ch Santosh Subudhi, S.R. Shimjith and A.P. Tiwari
Reactor Control Division

Abstract :

Advanced Heavy Water Reactor (AHWR), a natural circulation boiling water reactor, is reported to be prone to xenon instabilities. Xenon induced spatial instabilities are suppressed by the spatial power control program of AHWR. However, thermal hydraulic instabilities characterised by flow oscillations of the order of tens of seconds, are more challenging in terms of detection and control. In AHWR, the operating procedure is carefully formulated so as to avoid thermal hydraulic instabilities during start-up and operation. Nevertheless, the availability of an on-line monitoring mechanism to indicate the onset of such instabilities would aid the operator to monitor the operational state of the reactor and to take up immediate corrective measures in case of the onset of thermal hydraulic instabilities during unanticipated operating conditions. In this context, a time frequency representation based algorithm suitable for online implementation, is developed to detect the onset of the oscillations by continuous monitoring of the channel flow signals. Validation of the algorithm is carried out with data simulated using a homogeneous equilibrium model capable of demonstrating thermal hydraulic instabilities in the Main Heat Transport system of the AHWR.

Introduction

Advanced Heavy Water Reactor (AHWR) [1] is a 300 MWe, vertical, pressure tube type, heavy water moderated reactor which employs natural circulation of boiling light water for core cooling. The Main Heat Transport System (MHTS) of AHWR consists of four horizontal steam drums connected to common inlet header through downcomers. Fig.1 shows a simplified schematic of MHTS of AHWR showing a single heat transport loop consisting of a steam drum, downcomer, feeder, coolant channel and tail pipe. Subcooled light water is transported from the steam drum to the channel through the feeder originating from inlet header. Boiling takes place inside the channel and the resulting steam-water mixture is transported to the steam drum through the tail pipe.

AHWR, like many other natural circulation reactors, is prone to thermal hydraulic instabilities under certain operating conditions. It is reported that Ledinegg type instabilities (static in nature) and density wave instabilities (dynamic in nature) may occur in AHWR [1]. Ledinegg instabilities are suppressed in AHWR by operating at a high pressure (7 MPa). However, density wave instabilities can still be experienced if the operating conditions are not strategically controlled and therefore are of primary concern. Density wave instabilities manifest as flow oscillations of increasing

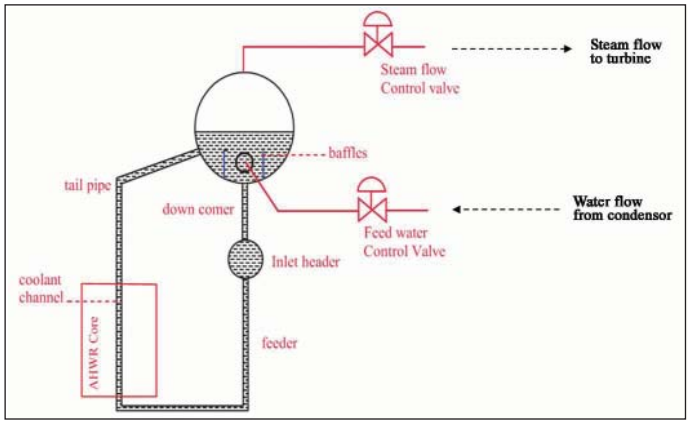

Fig. 1: Main Heat Transport System of AHWR (Schematic)

amplitude in response to any perturbation in system variables like flow, enthalpy, etc. These instabilities are caused due to multiple regenerative feedback effects between the flow-rate, vapour generation rate and pressure drop. Under certain operating conditions the feedback tends to become out-of-phase with a perturbation and results in self-sustained oscillations. In any natural circulation based reactor operating at a constant power, the fission power and core inlet subcooling essentially govern the stability conditions [2]. In AHWR, the core inlet temperature is varied (by controlling the feed water temperature) based on the operating power so as to avoid density wave instabilities during normal operation of the reactor. However, availability of real time stability information at the operator's console is still very beneficial to ensure smooth operation.

Nature of Density Wave Instabilities

It is necessary to study the effect of power and core inlet subcooling on the flow oscillations caused due to density waves instabilities. Density wave instabilities are simulated for a given combination of power and core inlet subcooling by initially maintaining steady state conditions and then introducing a small perturbation in power. For an unstable combination of power and core inlet subcooling, this perturbation leads to unstable oscillations in flowrate, density, pressure and enthalpy. The frequency of the flow oscillation is computed by studying the amplitude spectrum of the channel flowrate signal. The amplitude spectra of a time-domain signal can be obtained by carrying out a Fourier transform of the given signal. Fig.2 and 3 show comparison of normalised channel flowrates during onset of density wave instabilities and their single sided amplitude spectra at different powers and core inlet subcooling values respectively. The figures clearly indicate that the frequency of oscillation tends to increase with increasing power and decrease with increasing core inlet subcooling.

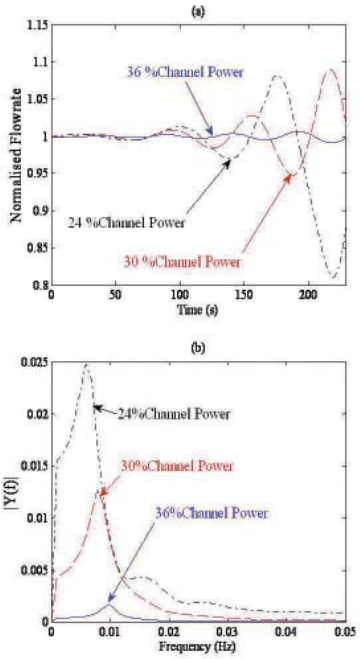

Fig. 2: (a) Normalised response of channel flow-rates at different power levels to a perturbation in power at a fixed inlet subcooling of 24K, (b) Single sided amplitude spectra (|Y(f)|) of the normalised channel flowrates

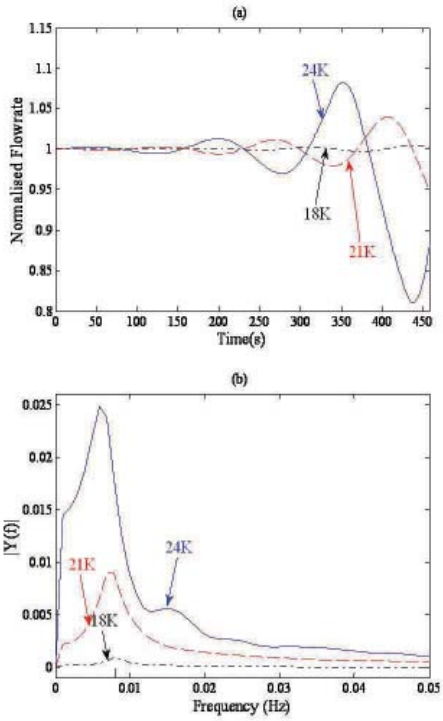

Fig. 3: (a) Normalised response of channel flow-rates at different core inlet subcooling to a perturbation in power around the operating power level of 24% channel power, (b) Single sided amplitude spectra (|Y(f)|) of the normalised channel flowrates

Similarly, it can also be observed that the amplitude of oscillation tends to decrease with increase in fission power and increase with increase in core inlet subcooling. These observations indicate that the frequency of density wave instabilities vary with time and are determined by the instantaneous operating condition.

Detection of Density Wave Instabilities

In boiling channel systems, density wave instabilities are undesirable as they may cause mechanical vibrations, system control problems etc [3]. In some cases they may rupture the heat transfer surface due to boiling crisis (dry-out, burnout) [2]. In AHWR, the design methodology is formulated to avoid such phenomena. Nevertheless, it is necessary and advisable to detect the onset of these instabilities during plant operation and make this information available to the operator. The onset of these instabilities can be detected by continuously acquiring the channel flow signals and sensing the presence of oscillations, followed by computation of the decay ratio of these oscillations. Decay ratio is defined as the ratio of two consecutive maxima of the impulse response. Decay ratio greater than unity would mean an unstable scenario, a value less than unity would mean a stable scenario. The simplest approach to compute the decay ratio could be to detect the magnitude of peaks of the oscillations whenever they appear and then compute the ratio of magnitude of present peak to that of the previous peak. However, this approach is not practical since the frequency of oscillation tend to vary with time. This problem can be addressed by using a time-frequency framework to describe the time varying flow signals rather than a conventional time-domain approach. A Time Frequency Representation (TFR) [4] gives the distribution of energy of a signal in time-frequency plane. The most widely TFRs are Short-time Fourier transform and Wigner-Ville distribution. However, in this work Wigner-Ville representation is preferred owing to its mathematical simplicity and the adaptability for real time applications. Fig.4 shows the Wigner-Ville time frequency distribution for a typical signal with linear variation in frequency. An algorithm based on Wigner-Ville time frequency representation is employed to predict a quantity called Instantaneous Decay Ratio (IDR) which would serve as a real time stability parameter. The algorithm also computes Accumulated Decay Ratio (ADR) defined as the accumulative multiplication of IDRs (in time) which projects the long term stability trend of the reactor.

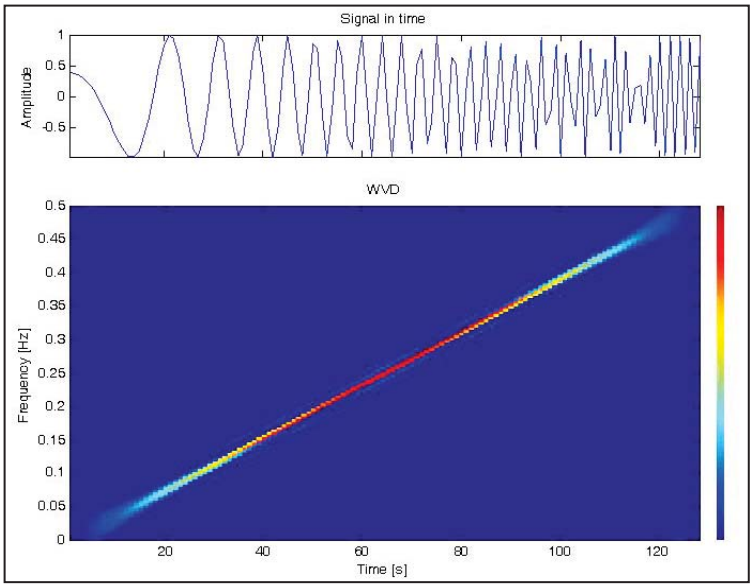

Fig. 4: A signal with linear frequency modulation (above) and WVD of the signal (below).

Algorithm for Computation of Decay Ratios

Fig.5 shows the schematic representation of the proposed algorithm which computes of IDR and ADR based on MHT channel flow information acquired at discrete time instants and infers about instability. The real signal sequence is converted

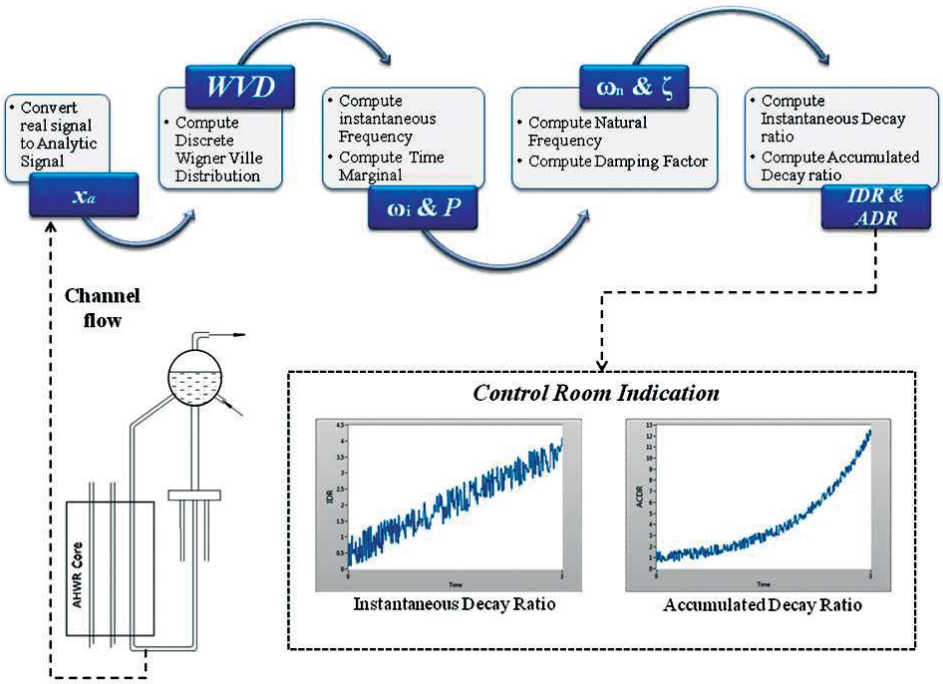

Fig. 5: Time frequency based algorithm for computing decay ratio

into analytic signal by removing the negative frequency components from the Fourier transform of the real signal and doubling the positive frequency components. Inverse transform of the resultant spectrum gives the analytic signal. It may be noted that conversion of the real signal into an analytic signal is necessary to eliminate the low frequency artefacts which appear in the Wigner time frequency distribution otherwise. The signal is then transformed into a zero mean signal and it is used to compute the Wigner-Ville time frequency distribution (WVD). The WVD involves FFT operation on the local autocorrelation of the analytic signal (localised product of time shifted signal at each discrete time instant). Instantaneous frequency (normalised first moment of frequency) is computed by taking the frequency weighted average of the magnitude of WVD at each discrete time instant. Time marginal (instantaneous power of the signal) is computed by adding the magnitude of WVD at each discrete time instant and multiplying the sum with the frequency resolution of the system. The natural frequency is computed using instantaneous frequency and the time marginal. The damping factor (computed from the natural frequency and time marginal) is used to compute IDR. The ADR is the accumulative product of local IDRs.

Online implementation

The proposed algorithm is suited for online implementation on a computer based system. The channel flow information can be sampled and acquired periodically, say every second, by a data acquisition module. A moving window (of width 200 s) of channel flow signal with certain degree of overlapping (of width 5 s) is fed to the algorithm and the decay ratios based on latest window of the flow signal are computed and continuously displayed on the operator console.

Validation of the algorithm

The effectiveness of the decay ratio based algorithm for instability detection is established using simulated channel flow data for various stable and unstable

scenarios obtained using a one-dimensional finite difference based homogenous equilibrium model of the MHT loop of AHWR, consisting of a single downcomer, tailpipe, boiling channel and riser. The model consists of mass, momentum and energy balance equations to represent the dynamics of coolant flow in the MHTS. It is assumed that there is no relative velocity between the two phases and the vapour and liquid in the channels and the riser sections are in thermodynamic equilibrium. Control volume-based spatial discretization and forward difference scheme discretization in time are employed to derive the difference equations for mass, momentum and energy conservation for various meshes in the MHTS. For a given operating power and core inlet subcooling, the steady-state distribution of system variables pressure, enthalpy, density and flow are computed using steady state equations. With the steady-state distribution as the starting point, time-dependent difference equations are solved for each mesh during transient conditions. A small perturbation is introduced in the channel power and the response of the system variables - pressure, enthalpy, density and flow is observed.

Fig.6 and Fig.7 show the preprocessed channel flow (converted into a zero mean signal), respective instantaneous decay ratios and accumulated decay ratios computed by the algorithm during the onset of stable and unstable oscillations respectively. Fig. 6 shows that the IDR value remains below unity indicating an instantaneous stable behaviour. The ADR shows a gradually decreasing trend showing a globally stable behaviour. Similarly, Fig. 7 shows that the IDR value remains above one indicating unstable behaviour throughout the time window and the ADR value gradually increases showing a globally unstable behaviour. The figures indicate that the decay ratio based algorithm effectively operates on the channel flow signal and gives the stability information of the system.

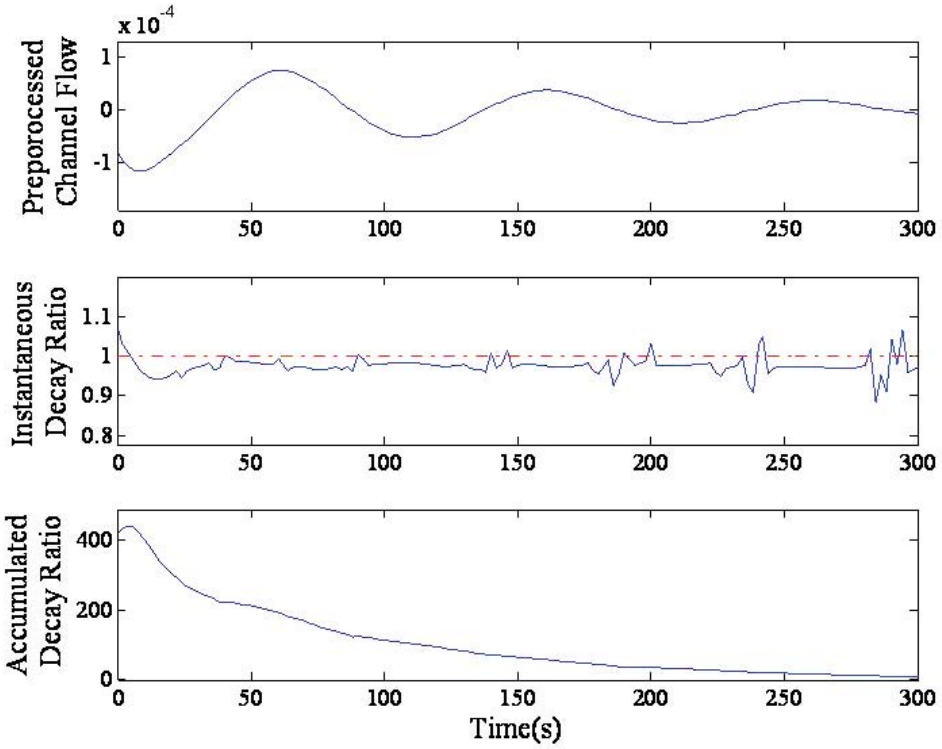

Fig. 6: Pre-processed Channel flow signal for a stable case of 24%Channel Power and core inlet subcooling of 12K and the time-variation of Instantaneous Decay Ratio and Accumulated Decay Ratio.

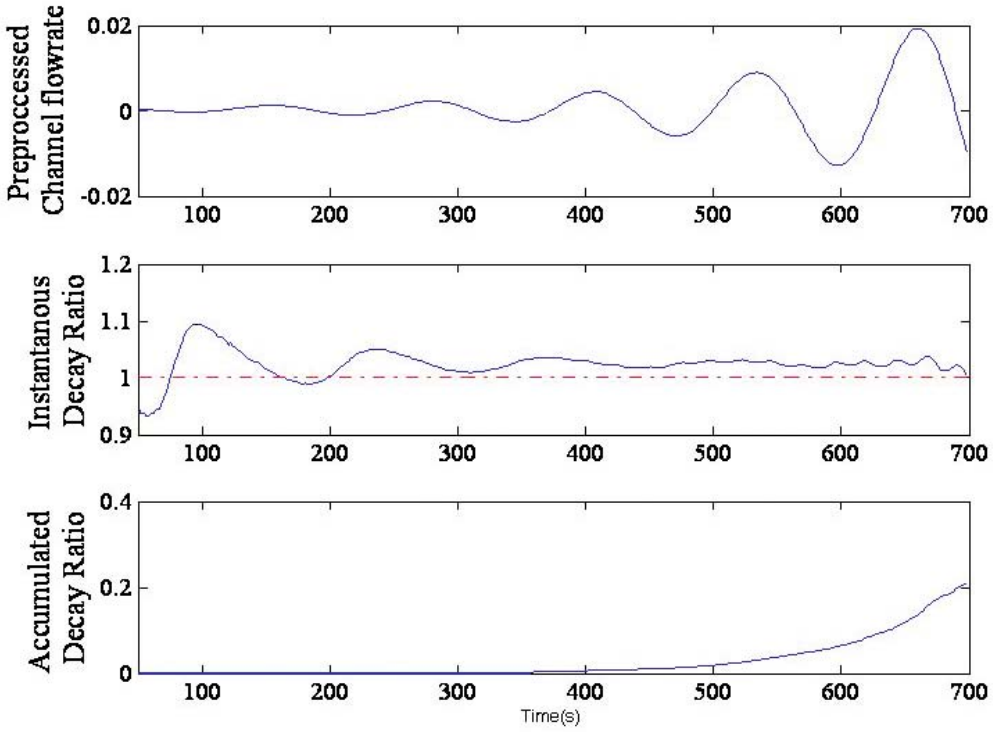

Fig. 7: Pre-processed flow signal for an unstable case of 24%Channel Power and core inlet subcooling of 18K and the time-variation of Instantaneous Decay Ratio and Accumulated Decay Ratio.

Conclusion

The decay ratio estimation based on Wigner -Ville time frequency representation is employed to devise an algorithm capable of handling time-varying nature of the density wave instabilities. The algorithm is found to be very effective in providing the stability information of the system during stable and unstable scenarios simulated using a homogenous equilibrium flow model. The algorithm is suitable for online implementation due to its computational simplicity. Implementation of this algorithm on hardware with real time data acquisition and computational capabilities would yield a system that is capable of indicating the stability status of the AHWR in real time. Such an instability monitoring system would be of immense benefit to the plant operator in taking up immediate corrective measures in the event of onset of instabilities.

References

1. Sinha R.K., Kakodkar, A. Design and development of AHWR- the Indian thorium fuelled innovative nuclear reactor. Nuclear Engineering and Design 236 (2006):683-700.
2. Boure, J.A., Bergles, A.E., and Tong, L.S. Review of two-phase flow instability, Nuclear Engineering and Design 25, (1973): 165-192
3. Su Guanghui et al. Theoretical and experimental study on density wave oscillation of two-phase natural circulation of low equilibrium quality Nuclear Engineering and Design 215, (2002): 187–198.
4. Cohen, L. Time Frequency Analysis. Prentice Hall, Eaglewood Cliffs, NJ, 1995.
5. Torres-Fernandez J.E. et al. Decay ratio estimation based on time frequency representations. Annals of Nuclear Energy, 37 (2010): 93-102.

Under Sodium Ultrasonic Imaging System for PFBR

V. H. Patankar, S. K. Lalwani, A. A. Agashe, G. D. Randale, R. Chaurasia, P. Jyothi, L.V. Murali Krishna, R. K. Jain, S. Srivastava, T. S. Ananthakrishnan, C. K. Pithawa
Electronics Division, BARC

Abstract

Under Sodium UltraSonic Scanner (USUSS) has been developed to detect the growth and protrusion of Fuel Sub-Assemblies of PFBR, submerged in liquid sodium by using the ultrasonic imaging technique during reactor shut-down when liquid sodium is at 180^{0}C. The imaging is carried out prior to every Fuel handling operation. Electronics Division, BARC has designed and developed an 8-Channel Ultrasonic Imaging System (UIS) which consists of 4 downward viewing and 4 side viewing ultrasonic transducers alongwith pulser-receiver, signal processing electronics hardware and software. An automated mechanical scanner developed by IGCAR houses sodium immersible transducers to image the fuel Sub Assemblies. The system has been successfully tested with dummy protruding and grown FSAs, submerged under liquid sodium. Such ultrasonic imaging systems are not available to India from international market. The USUSS developed indigenously has all the features available in similar systems developed by other countries.

After every imaging campaign, the mechanical scanner containing ultrasonic transducers is stored in the Argon filled storage-pit. Before every campaign of USUSS, it is necessary to check the healthiness of the sodium immersible and contaminated ultrasonic transducers, as the under-sodium scanner is decontaminated once in five years. For this purpose, a novel Non Contact Ultrasonic Inspection System (NCUIS) has been designed and developed by Electronics Division, BARC to check the functionality of the high-temperature and contaminated transducers of USUSS, using air-coupled ultrasonic technique.

Introduction

PFBR is a sodium cooled pool-type nuclear reactor which has sodium-submerged 181 Fuel Sub Assemblies (FSAs). During normal operation of the reactor, the temperature of liquid sodium is more than 550^{0}C. Due to high temperature, prolonged irradiation and flow of liquid sodium, there is a possibility of growth and protrusion of hexagonal shaped FSAs. As ultrasonic imaging technique only can be used for visualisation inside the optically opaque liquid sodium at 180^{0}C, an automated Under Sodium UltraSonic Scanner (USUSS) has been designed & developed for detection of growth and protrusion of in-core FSAs. Ultrasonic Pulse-Echo (PE) mode and C-Scan imaging technique have been used for this application. Sodium-compatible 5MHz ultrasonic transducers are employed for downward viewing operation for detection of growth in FSAs which are located underneath the scanner and 1MHz transducers are utilised to scan in sideways i.e. in lateral direction for detection of protrusion of FSAs. The scanning is carried out before every fuel handling operation so that Large and Small Rotatable Plugs of Prototype Fast Breeder Reactor (PFBR) can be rotated safely.

Core-plenum is a general level of all the in-core FSAs of PFBR. Detection of growth and protrusion of FSAs is to be carried out with reference to this level. For detection of growth in FSAs, maximum distance between the core-plenum and the front face of DVTs would be 100mm with minimum detection of growth to be 5mm. Therefore to meet this requirement, optimum frequency found out by experiments for DVTs is 5MHz. Similarly, to detect minimum 50mm protrusion of FSAs at a distance of 5m in sodium, optimum frequency found out by experiments for SVTs is 1MHz.

After completion of imaging campaign, the mechanical scanner is taken out of reactor vessel and stored in the Argon filled storage-pit. Before starting of every campaign of USUSS, it is necessary to check the health of all the ultrasonic transducers. These transducers, which have residues of sodium and are contaminated, are checked using air-coupled ultrasonic technique which does not require any liquid or solid couplant. The transducers are checked by pairing each of them with corresponding air-coupled transducers and each pair works in Transmit-Receive (T-R) mode. 16-Channel ultrasonic instrumentation designated as Non-contact Ultrasonic Inspection System (NCUIS) has been designed and developed for this purpose. Following description provides details of both the systems as well as their configuration, calibration setup and test results.

Under Sodium UltraSonic Scanner (USUSS)

System Description: Under Sodium Ultrasonic Scanner of PFBR comprises of Instrumentation & Control (I&C) H/W, system S/W and automated mechanical scanner. The I&C hardware of USUSS has been configured into 19" Control & Drive Panel and Ultrasonic Imaging System (UIS) Panel. The system software performs automated data acquisition, display, storage and analysis of 1D,2D,3D data/ images. Fig. 1 shows schematic block diagram of I&C of USUSS.

Ultrasonic Imaging System: The Ultrasonic Imaging System comprises of 8-Channel Ultrasonic Pulser-Receiver unit, Industrial PC with high speed PCI digitizer and system S/W and HV & LV DC power supplies. The pulser-receiver unit sequentially excites the ultrasonic transducers of USUSS using high voltage square wave tone-burst pulser; receives the reflected echo signals for each channel; amplifies and multiplexes them. The multiplexed echo signal is fed to PCI based 100MSPS, 8 Bits Digitizer located in PC. The software acquires, stores, processes and analyzes the data. The data acquisition is synchronized by generating suitable trigger signals within the pulser-receiver unit and the multiplexed trigger signal is connected to the Digitizer. Configuration of pulser-receiver

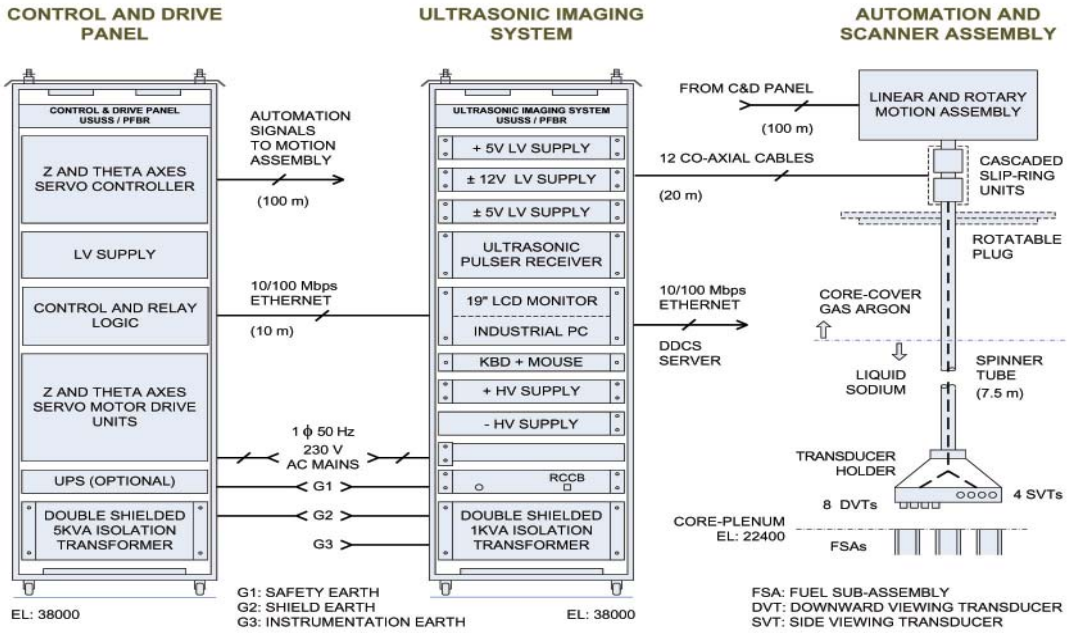

Fig.1: Schematic Block Diagram of I&C of USUSS for PFBR

Fig.2: 8-Channel Ultrasonic Imaging System

for deciding the no. of cycles in the tone-burst, frequency of excitation signal, receiver (amplifier) gain, band-pass filter selection, total channels etc., is achieved using RS232 interface between UPR unit and PC. Pulser-receiver diagnostics are performed to check availability of all LV DC power supplies, delivery of trigger commands, checking of active channels, checking of initial ringing of transducer/ reflected echo and filter settings etc. Fig.2 shows the photograph of 8-Channel Ultrasonic Imaging System. The system hardware has been qualified for Environmental compliances as per IS 9000 standards and EMI/EMC compliances as per IEC 61000 standards.

The Control and Drive (C&D) panel houses electronics hardware for controller of vertical (z) and rotational (θ) movements of the mechanical scanner. PC receives the Z and θ values from C&D panel over Ethernet.

Automated Mechanical Scanner and C&D Panel: 2-axes automated mechanical scanner has been designed and developed by IGCAR. Lower part of the scanner has 7.5m long spinner tube welded to a conical shaped transducer holder at the bottom-most position, containing 4 Downward Viewing Transducers (DVTs), 3 Side Viewing Transducers (SVTs) and 3 Spare DVTs. By imparting linear (Z) and rotary motion (θ) to the spinner tube, transducers are manoeuvred for imaging of FSAs. Upper part of scanner has Z & θ motors, ball-screws, Gear-box, feedback elements and slip-ring units to avoid entanglement of co-axial cables.

The C&D panel houses 2-axes AC servo motor controller and drives, control logic and Ethernet connectivity to PC for automated imaging.

System Software: QT-based Linux (Fedora-8) system-software has been designed & developed by ED, BARC for ultrasonic data acquisition, display, processing/ analysis, automation control, UPR configuration, diagnostics and interface to Distributed Digital Control System (DDCS) server for data/image archival and fetching co-ordinates of rotatable plugs of PFBR. Image processing/ analysis includes C-Scan imaging, growth monitoring of FSAs using DVTs and detection of protrusion of FSAs using SVTs, TOF/distance measurement and comparison with base-line data/image. The system software installed in the PC of UIS, controls the overall operation of USUSS. Before initiating the imaging of FSAs either by DVTs or by SVTs, 1D A-Scan waveform data is utilised to set time gates along the time or depth axis with user selectable amplitude threshold, so as to acquire 3D C-Scan image data of region- of-interest. As H/W based passive bandpass filters have been utilised for SNR enhancement of ultrasonic signals, separate digital filtering/ processing techniques have not been applied on image data. The main goal of USUSS is to view the in-core sodium-submerged FSAs of PFBR for detection of their relative growth and protrusion with reference to core-plenum. Frequency analysis of stored data has not been at present carried out.

Under-water Test Setup for Calibration of UIS:

Under-water test set up has been fabricated and installed at ED, BARC for the calibration of 8-Channel Ultrasonic Imaging System. 10m long pipe-assembly set-up is shown in Fig. 3a. The horizontally placed pipe assembly was filled with water. A circular opening has been provided to mount the 1MHz SVT at one end of the pipe-assembly and a rectangular cut-out has been provided at the other end of pipe to place cluster of 10 FSA top-heads made of SS as shown in Fig. 3b. FSA top-heads (each 90 mm tall) and reflector sub-assemblies (3 nos. of each having 88 mm OD and 190 mm height) were placed over the flat plate resting inside the pipe.

Fig. 3a: 10 m Long Pipe Assembly

Fig. 3b: Cut-outs for Transducer and FSA Top-heads in 10 m Long Pipe Assembly

The cylindrical reflector SAs were placed behind the cluster of FSA top-heads, with reference to face of SVT. Circular discs of thickness range 5-50mm were placed under one of the FSA top-heads to simulate protrusion. Provision was made to change the orientation of protruding FSA with respect to the front face of SVT. The detection of protrusion was carried out in under-water setup where the protruding FSA was kept at a distance of ~9 m from the front surface of SVT. Cluster of nine FSAs were placed at same level and were kept between the protruded FSA and SVT to form the core-plenum. The actual height of hexagonal shaped full-length FSA of PFBR is 4.5m whereas only 90mm tall top-heads, having identical shape as the original FSA with 3mm flat annular surface at the top of FSA, have been used for calibration of 8-Channel ultrasonic imaging system. To simulate the divergence of ultrasound in sodium, 10m pipe, filled with water was selected, to match the difference in acoustic velocities. Maximum distance to be scanned in PFBR would be ~5m in sodium.

Major parameters governing the fidelity of ultrasonic images are based on the axial resolution of the transducer, digitization rate and angular/ linear step size with which automated ultrasonic images are acquired. For imaging activity carried out by DVTs, the optimum angular step size found out by experiments is 1 degree whereas, for SVTs, the angular and linear step sizes found out by series of experiments is 1 degree and 2mm respectively.

Results of Under-water Testing:

8-Channel Ultrasonic Imaging System has been tested with varying amount of protrusion ranging from 5 mm to 50 mm as well as with two different orientations of the protruding FSA by placing flat surface or the edge of hexagonal shaped FSA in front of SVT. Distinct echo signals were obtained from FSA with 25mm or higher protrusion when its flat surface/ edge was facing SVT.

The amplitude of echo signal received from protruded FSA was observed to be increasing with increase in protrusion. Fig. 4 shows a typical A-Scan waveform obtained with 50 mm protrusion at a distance of around 9 m, in water. Also, irrespective of the orientation of protruded FSA, the echo

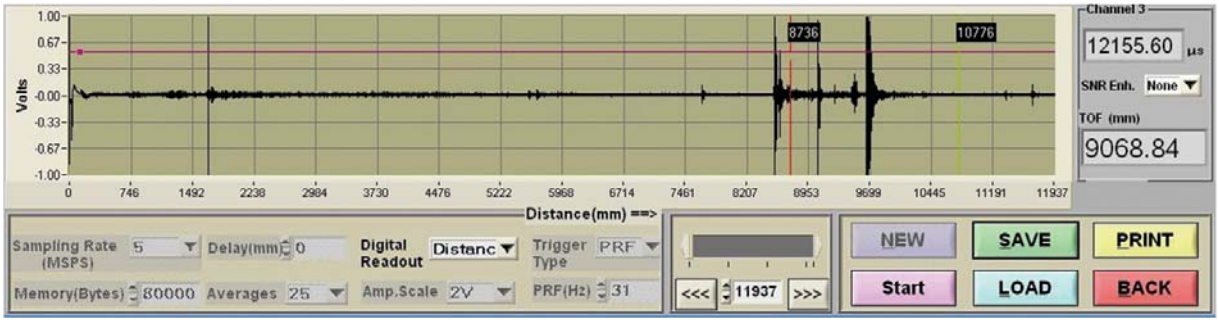

Fig. 4: Typical A-Scan Waveform Acquired for Detection of 50 mm Protrusion of FSA

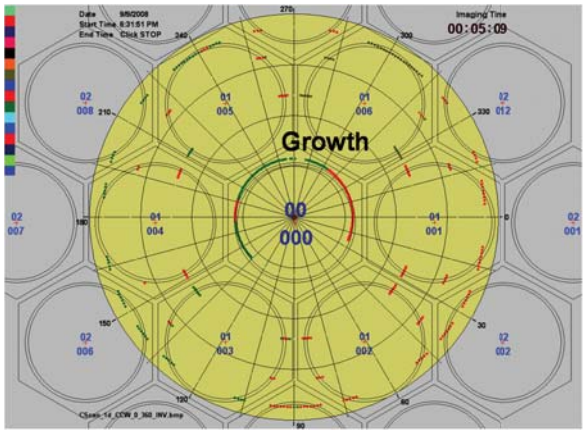

Fig. 5a: FSA Mapping using 4 DVTs

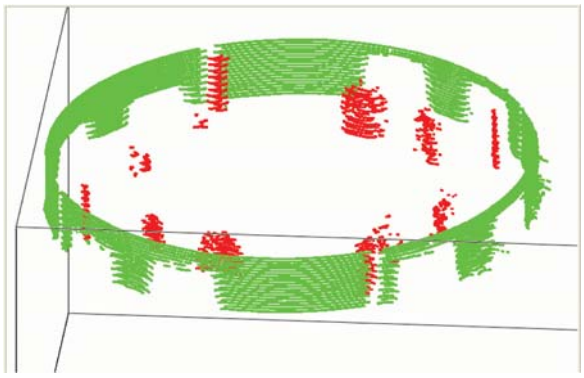

Fig. 5b: 3D Ultrasonic Image of FSAs using SVT

signals received from the cylindrical shaped reflector SAs were observed to have a trend of increase in amplitude with the reduction in protrusion from 50 mm to 25 mm.

Fidelity of echo signals was confirmed also by generating water flow of 1m/s in pipe setup and 10% reduction in echo signal amplitude was observed.

Results of Under-sodium Imaging: Prototype Ultrasonic Imaging System was tested in sodium test-vessel at IGCAR, Kalpakkam, Tamilnadu. The sodium vessel test setup comprised of 1m diameter tank containing 27 dummy FSA top-heads at the bottom-most position. 19 FSA top-heads were placed under the transducer holder and remaining 8 FSA heads were mounted along periphery of the tank at different orientations with reference to the face of SVTs. Fig. 5a shows the C-Scan image of 19 FSAs located underneath the transducer holder and detection of 5mm growth of one of the FSAs. Fig. 5b shows the 3D ultrasonic image of the setup indicating locations of tie-rods used to hold the test setup, and 8 FSAs with different orientations. The circular shaped image at the boundary shows the wall of the tank containing all the FSA top-heads.

16-Channel Non-Contact Ultrasonic Inspection System: The NCUIS is used to check the functionality of ultrasonic transducers of USUSS, without making any contact with the contaminated transducers, before every campaign of USUSS of PFBR. Instrumentation of 16-Channel NCUIS, housed in 19" rack, is based on air-coupled ultrasonics and works in T-R mode of operation. A test-jig consisting of 8 sodium-compatible and 8 Air-coupled transducers has been fabricated for testing of NCUIS. Each pair of the sodium-compatible and air-coupled transducer is placed along the line-of-sight with a known stand-off distance.

Initially, the sodium-compatible transducers were sequentially energized by a tone-burst pulser to transmit ultrasound in air and the corresponding air-coupled transducer of the same frequency was used as a receiver. The signal was amplified using programmable gain amplifier with gain more than 100dB. A-scan waveforms were recorded for off-line measurements. Subsequently, the role of each transducer within the pair was interchanged and data was once again recorded. The received signals for both the setup were (off-line) analyzed for the assessment of health of sodium-compatible and contaminated transducers for its sensitivity as a receiver, transmission capability as a transmitter and computation of frequency contents of the received signal. DVTs and SVTs are narrowband transducers and so the frequency analysis carried out on received signals was only for academic study.

The NCUIS is capable of driving four pairs of 1MHz transducers and four pairs of 5MHz transducers to check the healthiness of SVTs and DVTs of USUSS. T-R mode of inspection is used because the sensitivity of 5MHz transducers is not adequate to work in air using Pulse-Echo (PE) mode due to excessive attenuation of energy at higher frequencies in air.

Fig. 6: 16-Channel NCUIS System

NCUIS System Hardware: PC based 16-Channel NCUIS consists of 8-Channel Ultrasonic Tone-Burst Pulser with ±300V square-wave output and programmable 1-15 cycles of tone-burst; 8-Channel wideband receivers with programmable gain up to 120dB@ 10MHz (-3dB BW); 100 MSPS-8-bits PCI bus-based digitizer board located in Industrial grade PC, DC power supplies and an isolation transformer. Fig.6 shows the photograph of the system panel.

NCUIS System Software: GUI software has been developed for NCUIS. It facilitates A-Scan data acquisition, display and storage of 1D data, measurement of TOF/distance and frequency analysis of the acquired data.

Test Setup for Calibration of NCUIS and Results: The test-jig, fabricated for the purpose, comprises of four 5MHz ultrasonic transducers, representing DVTs of USUSS, facing 4 air-coupled ultrasonic transducers of same frequency with a stand-off distance of ~25 mm, as depicted in Fig. 7. Similarly 4 more 1MHz transducers, representing SVTs of USUSS, and corresponding 4 air-coupled transducers of same frequency were mounted on the test-jig with a stand-off distance of ~45 mm.

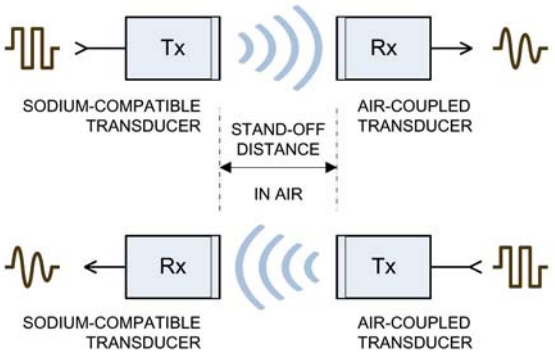

Fig. 7: Health-Checking of Sodium-Compatible Transducer as Transmitter and Receiver

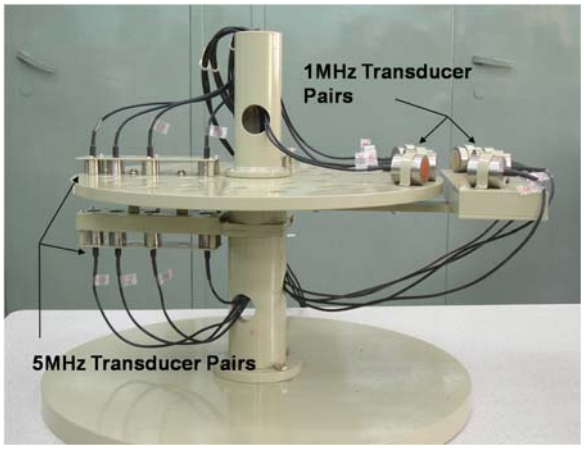

Fig. 8: Test-Jig for Calibration of NCUIS

The test-jig has been designed and manufactured by Workshop of ED, BARC and the photograph of test-jig is shown in Fig. 8.

NCUIS Test Results: The NCUIS system was connected to the transducers, mounted on the test-jig, using 20m long cables. The cables were routed through two slip ring units to simulate the actual connections of USUSS transducers of site. The received signals for 1MHz and 5MHz sodium-compatible transducers were recorded. Fig. 9a and Fig. 9b show the signals obtained from the 1MHz and 5MHz SVTs and DVTs respectively.

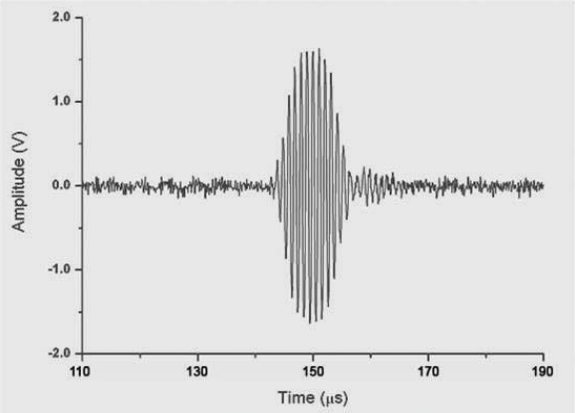

Fig. 9a: Signal received by 1MHz SVT

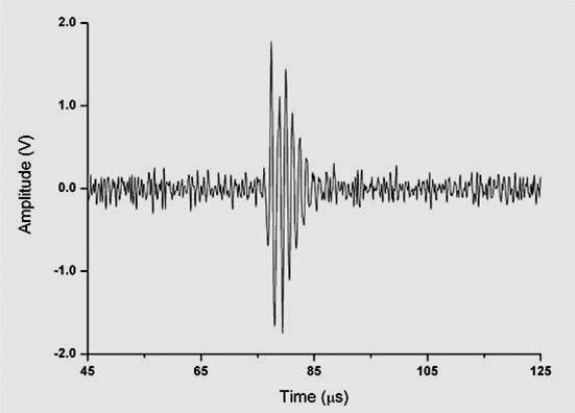

Fig. 9b: Signal received by 5MHz DVT

Conclusion

Two innovative systems namely, UIS and NCUIS have been designed and developed for USUSS of PFBR. The main function of UIS is to perform under-sodium ultrasonic imaging of PFBR core for detection of growth and protrusion of FSAs. Using sodium test vessel setup, 5MHz DVTs, 8-Channel UIS and an automated USUSS, 5mm growth of FSAs was detected. Using under-water 10m long pipe set-up, UIS and 1MHz SVTs, 25mm FSA protrusion was detected in water at a distance of 9m which is equivalent to ~5m in sodium. NCUIS is mainly intended for checking functionality of contaminated transducers of USUSS in the storage-pit area.

The pulse-echo technique based 8-Channel Ultrasonic Imaging System of USUSS has been completely tested using under-water test set-up at ED, BARC, Mumbai as well as in under-sodium test vessel at IGCAR, Kalpakkam, Tamilnadu for detection of growth and protrusion of dummy Fuel Sub Assembly top-heads.

The Non Contact Ultrasonic Inspection System, based on air-coupled ultrasound and working in T-R mode, has also been tested at ED, BARC. Both the above systems have been delivered to BHAVINI, Kalpakkam, TN.

Acknowledgement

Authors wish to acknowledge the support received from all the BARC and IGCAR team members of task-force for USUSS of PFBR.

Applications of Digital Reactivity Meter based on Kalman Filtering Technique in Indian Nuclear Reactors

R.K. Patil
Raja Ramanna Fellow, E&I Group
and
S.R. Shimjith
Reactor Control Division

Abstract

A reactivity meter based on Kalman filter algorithm is developed in Reactor Control Division, Bhabha Atomic Research Centre, for providing the reactor operator with a direct, online, real-time indication of the absolute reactivity status of the reactor core under all states of the reactor from shutdown through start-up to power operation. The reactivity meter has potential applications such as estimation of reactivity perturbations around critical conditions, indication of point of criticality during reactor startup, shutdown margin monitoring, worth computation and calibration of reactivity devices, detection of inadvertent insertion/ removal of reactivity under subcritical conditions etc., thereby improving the overall safety in reactor operation. This article summarizes the applications of the reactivity meter in Indian nuclear reactors, and its effectiveness in such applications as experimentally established. It also looks at the regulatory benefits and support to utility in economization of plant operation.

Introduction

In reactor operation or experiments, signals indicating reactor power (or neutron flux) and reactor period are generally used for direct information on the state of the reactor. However, the most important time dependent parameter is the reactivity, and in the past few decades, many techniques were proposed by researchers for on-line dynamic computation of reactivity from the above mentioned signals. Many nuclear reactors worldwide are equipped with such reactivity meters. Most of these digital reactivity meters employ reactivity estimation based on inverse point kinetic equations or otherwise based on reactor period. However, these algorithms demand an accurate knowledge of the model parameters, which is difficult to provide in many cases. Also they do not have any direct provision to eliminate noise content in the data, and hence fail miserably in estimation of subcriticality when the noise content in detector signal is large compared to the neutron flux level. This is where the Kalman Filtering algorithm, with its inherent ability to work with even highly noisy input signals and uncertain plant parameters, serves as a promising candidate.

The Kalman Filter is a recursive stochastic estimator algorithm, which uses a mathematical model of the process to predict the instantaneous values of all the process variables (in the form of a vector called the 'state'); including those which cannot be directly measured [1]. It further corrects these predicted values using a feedback of the error between the available measurements from the actual process and the predicted outputs, through an optimally computed feedback gain K. This predictive-corrective process, with in-built noise filtering capability resulting from the recursive optimal computation of the feedback gain, repeats in each cycle of the algorithm execution as shown schematically in Fig. 1.

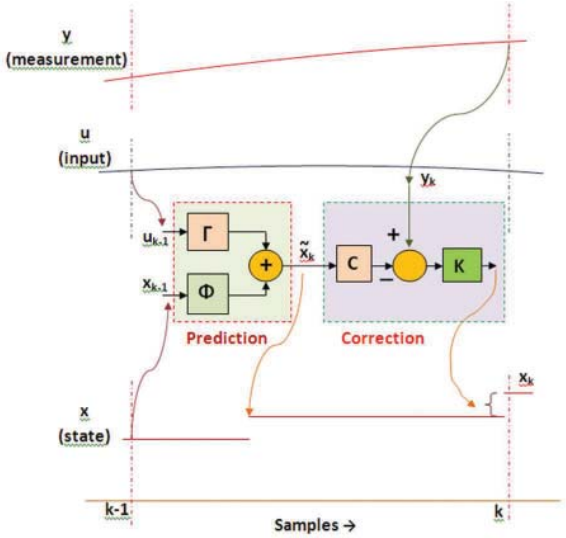

Fig. 1: Schematic representation of Kalman filter algorithm

A reactivity meter based on this algorithm is developed in Reactor Control Division, Bhabha Atomic Research Centre, for providing the reactor operator with a direct, online, real-time indication of the absolute reactivity status of the reactor core under all states of the reactor from shutdown through start-up to power operation, unlike the conventional reactivity meters effective only during power range operation [2]. The reactivity meter employs an embedded system hardware consisting of processor with add-on data acquisition and analog output cards. It accepts the signals corresponding to reactor power from the neutronic channels, and provides indication of the estimated reactivity through a dedicated Graphical User Interface (GUI) panel as shown in Fig. 2, and/or an analog meter mounted on the control panel in Main Control Room. The reactivity meter algorithm adopts the point kinetics model of the nuclear reactor in standard state space form, with neutron life time and delayed neutron data specific to the reactor as the design data [3]. In order to use the model for subcriticality indication, the source term is explicitly modeled in terms of a known initial stable subcriticality and corresponding steady state power level for any reference subcritical condition, which form two additional design parameters for the meter.

During the past decade, efficacy of this reactivity meter in estimation of core reactivity under different operating conditions has been demonstrated in various nuclear reactors. Vast operational experience from these exercises has proved that the meter is a very handy tool in applications such as estimation of reactivity perturbations around critical conditions and indication of point of criticality during reactor startup, shutdown margin monitoring, worth computation and calibration of reactivity devices, detection of insertion/removal of small amounts of reactivity under subcritical conditions etc. The applications of the reactivity meter in Indian nuclear reactors, and its effectiveness in such applications as experimentally established, are touched upon in the forthcoming sections.

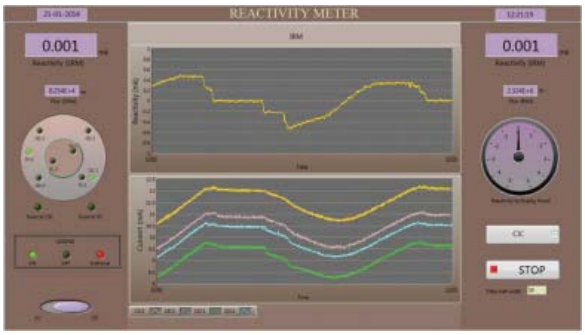

Fig. 2: Screenshot of the reactivity meter GUI

Indication of point of criticality during reactor startup

The reactivity meter can effectively be used during startup operation of nuclear reactors, including first startup, to monitor the approach to criticality. Fig. 3 shows the response of the reactivity meter during the first approach to criticality of a critical facility in Trombay. The meter had been indicating the instantaneous shutdown margin while withdrawing a control rod in small steps. As the rod approached its critical position, indicated reactivity also approached to zero. When the rod position attained 771 mm, the estimated reactivity was close to zero, indicating the criticality. Subsequently when the rod was driven further out and kept at 792 mm for about 5 minutes, it indicated a

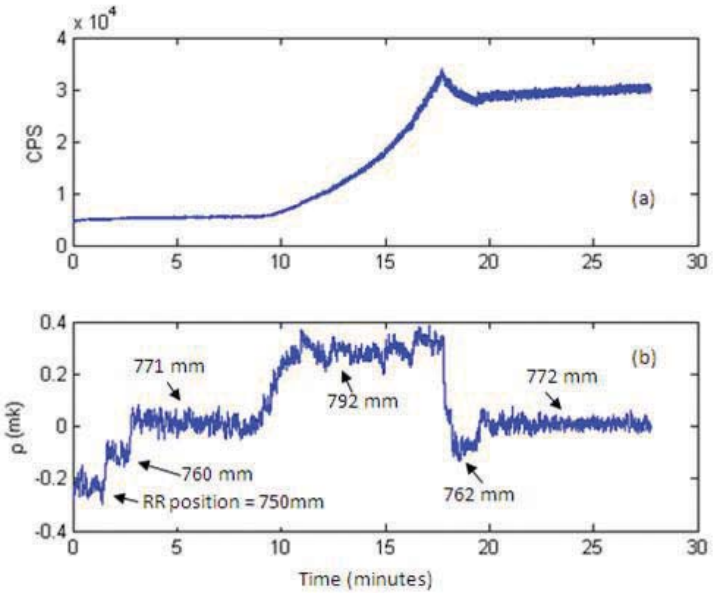

Fig. 3: Response of the meter during approach to criticality.

supercriticality of about 0.3 mk. During this phase, the reactor was declared critical. Afterwards the rod was driven down to 768 mm during which the indicated subcriticality was about -0.08 mk. Soon the rod was driven slightly out to 772 mm, on which the reactivity indicated was zero. Reactor was operated at critical steady state with the rod at 772 mm as shown.

Subcriticality Monitoring

Real–time indication of subcriticality is a challenging problem, essentially due to the difficulties in modeling the neutron source strength with sufficient accuracy, and also due to the high fluctuations in neutron signals measured in subcritical systems. The Kalman filter algorithm has inherent capability to work with stochastic signals and hence addresses the latter issue efficiently. Former issue is taken care of by an explicit modeling of the neutron source in terms of any known initial subcriticality as mentioned previously. Efficacy of the meter in indication of subcriticality has been validated in research reactors and critical facility at Trombay and in Fast Breeder Test Reactor (FBTR), Kalpakkam.

Fig. 4 depicts the performance of the meter in the critical facility during a transient involving lowering of control rod followed by dropping of safety rods. Prior to the transient, the meter indicated that the reactor was subcritical by about 2.9 mk. When the control rod reached core bottom, indicated subcriticality was about 7 mk. Subsequently when the shut off rods reached core bottom, the indicated subcriticality was stabilized at 63 mk. These figures were found to be in very good agreement with the values calculated by the reactor physicists. It is also established that the Reactivity Meter can indicate the reactivity even under a prolonged shutdown, thus providing valuable information of the shutdown margin of the reactor.

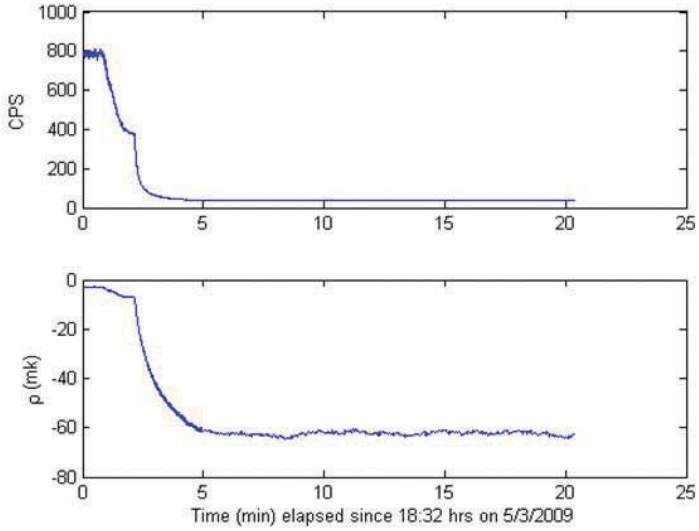

Fig. 4: Subcriticality indication in the critical facility during the lowering of regulating rod followed by reactor trip.

Worth Computation and Calibration of Reactivity Devices

Experiments conducted in different reactors demonstrate the capability of the meter to serve

as a handy tool for direct online computation of the worth of different reactivity devices and their calibration. Outcome of one such exercise in the critical facility is depicted in Fig. 5. It shows the worth estimation when two shutoff rods were withdrawn sequentially. With both the shutoff rods at core bottom, reactivity indicated was -90 mk. When first rod was fully retracted, it was about -57.75 mk which shows that its worth is 32.25 mk. When the second rod was fully withdrawn, reactor was still subcritical by about 31 mk. This indicates that the worth of the second rod, with the first one at top, is 26.75 mk.

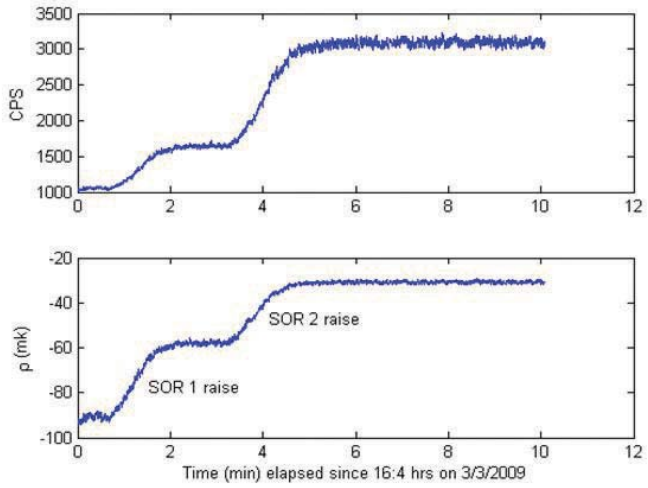

Fig. 5: Online estimation of shutoff rods' worth in critical facility.

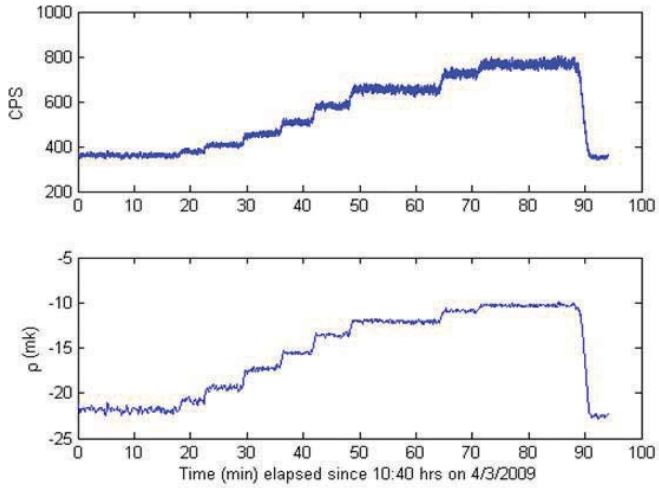

Fig. 6: Indicated reactivity during regulating rod calibration exercise in critical facility.

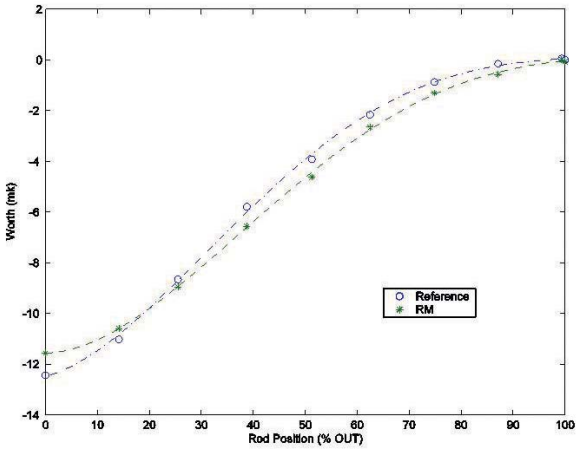

Fig. 7: Comparison of the calibration curves generated from reactivity meter readings and physics computations.

Likewise, Fig. 6 depicts the response of the meter during step by step withdrawal and subsequent insertion of the regulating rod in the critical facility. Prior to the withdrawal of the regulating rod, the indicated subcriticality was 22.6 mk. The regulating rod was withdrawn in steps of about 100 mm till it reached the core top when the subcriticality indicated was 10.8 mk. Hence, the worth of the rod as indicated by the reactivity meter is 11.8 mk, against the calculated worth of 12.6 mk. From the reactivity estimated by the meter at different rod positions, the calibration curve of the rod was plotted off–line. Fig. 7 compares this calibration curve, with that generated from the physics calculations.

Detection of reactivity changes during fuelling operations

The feasibility of using the reactivity meter for the purpose of measuring the reactivity during shutdown, fuel handling and startup of the reactor was established in FBTR. Measurement of reactivity during fuel handling operations was of prime significance. During the fuel handling campaign, various fuel sub assembly transfer operations were carried

out. While transfer operation is in progress the changes in core reactivity values were estimated online by the reactivity meter. From the results obtained, it was concluded that the meter is very effective in indication of the worth of fuel pins. Subsequently it was proposed to connect the meter as a diverse measuring instrument to the existing reactivity meter which is effective only in the high power range. Fig. 8 depicts the response of the meter during this fuel handling operation, which indicates that the meter recognizes each incident of fuel pin removal / insertion, and provides a direct indication of the worth of individual pins.

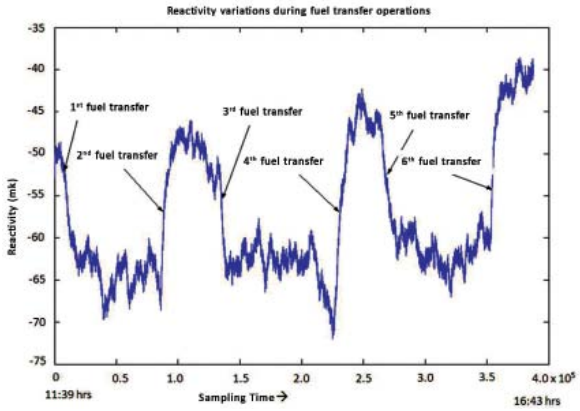

Fig. 8: Response of the meter during fuel handling operations in FBTR.

Drop Time Monitoring of Safety Rods

In PFBR, there are two independent, fast acting, and diverse shutdown systems, the first comprising of nine Control & Safety Rods (CSRs) and the second consisting of three Diverse Safety Rods (DSRs). Monitoring of the drop-time performance of the DSRs is an important design requirement, however, design does not provide for direct sensing of top and bottom positions of DSRs due to physical restrictions on layout and unfavorable environmental conditions. Therefore, the drop time of DSRs will be monitored in PFBR using the reactivity meter, based on the principle that the drop-time can be found out from the record of reactivity change subsequent to the dropping of

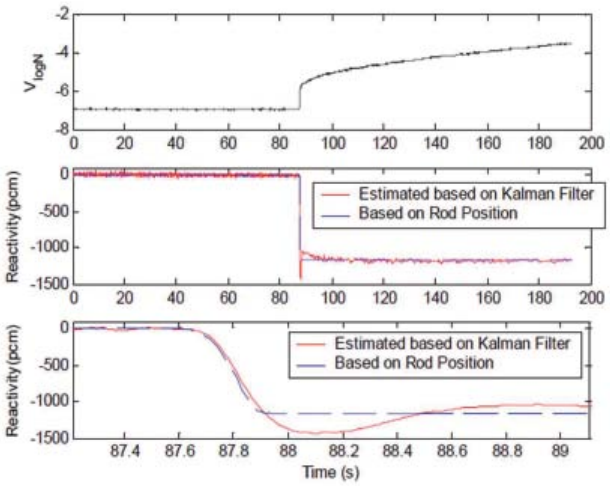

Fig.9: Estimated and actual reactivity during a rod drop in FBTR

the rods since the change in reactivity status of the core on shut-off rod drop is equal to the worth of the shut-off rod. The efficacy of the reactivity meter in estimation of rod drop time has been demonstrated through offline analysis as well as rod drop experiments in FBTR. Fig. 9 depicts the time variations of neutronic signal, estimated reactivity and the reactivity computed from the rod position, during dropping of a shutoff rod in FBTR. The deviation between rod drop time inferred from the reactivity values estimated by the reactivity meter and the drop time inferred from rod position signal is found to be less than 20 ms, which is considered acceptable for sensing of rod drop time [4].

Concluding Remarks

The applications of the reactivity meter based on the Kalman filtering technique have generated remarkable confidence in its usage. The reactivity meter facilitates continuous surveillance of the core reactivity status from shutdown through the start-up and power range operation of the reactor. Since it always indicates the true state of the reactor, shutdown margin is always directly known, and not inferred by status of reactivity devices as it happens in PHWRs today. The meter assists the operator in monitoring the shutdown margin, detection of any inadvertent introduction of reactivity into the core and in assessment of any requirements of addition

of boron in the moderator, thereby improving the overall safety in reactor operation.

There is generally a stipulation by regulator that Minimum Shutdown margin of 10 mk must be maintained during shut down at all times. There are no means available in Indian reactors to verify this stipulation. Hence it is always up to utility to show the regulator by calculations that this stipulation is being met. The situation becomes even more complicated when the reactivity in the reactor can change substantially due to change in temperature and Xenon concentration. If an online reactivity meter is installed in the plant it provides direct monitoring of the reactor status, thus enabling regulator o monitor the specified Shutdown margin criterion.

The Reactivity Meter can offer the best protection against inadvertent criticality happening in a nuclear reactor. Reactivity Meter can be used to generate an alarm whenever Reactor keff exceeds 0.99 or is within 10 mk of becoming critical. This indirectly provides regulatory benefits by improving safety.

Specification of shutdown system is often made in terms of speed of actuation of device i.e. Shutoff rods insertion time or injection time in case of liquid poison system. These are again indirect means of ensuring safety, true parameter for reactor being the negative reactivity insertion time. With the reactivity meter regulator can now insist on measure of negative reactivity insertion time.

The reactivity meter can effectively provide a direct estimate of the variations in xenon load subsequent to a reactor trip. This will aid the operator in restarting the reactor prior to a poison out, or in delay of boron addition to maintain adequate Shutdown margin and will also provide more time to the utility whereby it can optimize the amount of boron to be added; in fact in most of cases the plant may be able to skip the boron addition completely. This provides two benefits, first, it will reduce load on resin used in boron removal system which will reduce the radioactive waste. Second, it will reduce the startup time for the reactor as boron removal time will be reduced drastically in most of the cases.

The capability of the reactivity meter in online monitoring of sub criticality status of the reactor cores can be exploited to extend its application to the monitoring of spent fuel storage pools. With dedicated neutron detectors strategically located inside the spent fuel storage pools, sub criticality status of the pools can be monitored continuously thereby enhancing the safety of the storage pools.

Finally, it is convincingly felt that a reactivity meter is a very useful and convenient instrument for reactivity measurements during the physics experiments. It provides direct reactivity measurement in many experiments with great convenience and accuracy, which would not be possible through conventional means.

Acknowledgement

The authors express their sincere gratitude to Director E&IG and Director RPG, BARC, and Director ROMG, IGCAR for their kind support.

References

1. H. W. Sorenson, "Kalman Filtering Techniques," Kalman Filtering: Theory and Application, edited by H. W. Sorenson, New York: IEEE Press, 90 - 126 (1985).
2. A.P. Tiwari, B.R. Ivan. "Kalman Filtering Technique for Reactivity Measurement". Proceedings of symposium on Advances in Nuclear and Allied Instrumentation (SANAI - 97), Feb 5-7, 1997, BARC.
3. T.U. Bhatt, S.R. Shimjith and A.P. Tiwari, "Estimation of shutdown reactivity in power reactor: Comparative study of inverse point kinetics and Kalman filtering," BARC Newsletter, Issue No. 324, Jan-Feb 2012.
4. Report of the task force for the development and supply of Kalman filter based system for monitoring the drop-time performance of PFBR-DSRDM.

Measurement of Internal Diameter of Pressure Tubes in Pressurized Heavy Water Reactors using Ultrasonics

Manojit Bandyopadhyay, Amit K Haruray, A.M. Kadu, Gurpartap Singh, H.M. Bapat, M. Padmanabhan, R.K. Puri and D.N. Badodkar
Division of Remote Handling & Robotics

Abstract

The Pressure Tube in Pressurized Heavy Water Reactors (PHWRs) undergoes dimensional changes due to the effects of creep and growth as it is subjected to high pressure and temperature, which causes Pressure Tubes to permanently increase in length and diameter and to sag because of weight of fuel & coolant (heavy water) contained in it. These dimensional changes are due to prolonged stresses under high temperature & radiation. Pressure Tube stresses are evaluated for both beginning and end of life for accounting the Pressure Tube dimensional changes that occur during its design life. At the beginning of life, the initial wall thickness and un-irradiated material properties are applied. At the end of life, Pressure Tube diameter and length increases, while wall thickness decreases. Material strength also increases during that period. The increase in Pressure Tube diameter results in squeezing of garter spring spacer between the pressure and calandria Tubes. It also causes unacceptable heat removal from the fuel due to an increased amount of primary coolant that bypasses the fuel bundles. This reduces the critical channel power at constant flow. Hence the periodic monitoring of pressure Tube diameter is important for these reasons. This is also required as per the applicable codes and standards for In-Service Inspection of PHWRs. Mechanical measurement from ID of the Tube during periodic monitoring is not practically feasible due to high radiation and inaccessibility. This necessitates the development of NDT technique using Ultrasonics for periodic in-situ measurement of ID of pressure Tubes with a BARC made remotely operated drive system called BARCIS (BARC Channel Inspection system). The development of Ultrasonic based ID measurement techniques and their actual applications in PHWRs Pressure tubes are being discussed in this paper.

Key Words: Ultrasonic velocity, Heavy water, In-situ Calibration, Stepped reference block, Coolant Channel

Introduction

The Pressure Tubes in Pressurized Heavy Water Reactors (PHWRs) undergo dimensional changes due to the effects of irradiation creep and growth. This causes permanent increase in length and diameter of pressure Tube and also sag that occurs from the weight of the fuel bundles and coolant contained in it. The increase in diameter may lead to fuel failure due to in-sufficient cooling caused by the coolant bypassing the fuel bundle. Squeezing of garter spring spacer between the pressure and Calandria Tubes may create safety issues. The coolant bypassing the fuel bundles also reduces the critical channel power at constant flow. Thus, the diameter expansion turns out to be a major life limiting parameter for the reactor Pressure Tubes. Hence periodic monitoring of pressure Tube diameter is necessary during In-Service Inspection (ISI) and also during pre-service inspection (PSI) for baseline data. Mechanical measurements from inside the Tube are difficult due to high radiation and inaccessibility. The presence of heavy water as coolant helps the use of Ultrasonic immersion based techniques for periodic

in-situ measurement of Internal Diameter (ID) for pressure Tubes along with a remotely operated drive system (BARC Channel Inspection System) BARCIS. Since the Ultrasonic velocity is highly dependent upon temperature of the medium, in which they are travelling; a provision has been made for in-situ compensation for velocity variation in heavy water flowing through PT under measurement. This paper describes the development of UT based two techniques viz. full wave rectified flank method & negative half wave rectified peak method for PT ID measurement with in-situ ultrasound velocity compensation required to maintain measurement accuracy. It also discusses our experiences gained during ID measurements carried out at different reactors (for both types of PHWRs; 220MWe & 540 MWe PHWRs).

EXPERIMENTAL SET UP:

BARCIS Inspection head for ID measurement has been designed with three 10 MHz immersion spot focused probes; two probes are used for measurement of water path kept at diametrically opposite to each other (180° apart) and the third probe is used for calibration, kept at a fixed distance from a stepped reference reflector as shown in Fig 1. First ID is measured at 12 locations of the reference standard piece where it is mechanically measured using two axis co-ordinate measuring machine (CMM) and the calibration is done using calibration probe and stepped reference reflector by observing the difference between first and second echo using digital Ultrasonic flaw detector having multiple gates and minimum reading accuracy 0.01 mm (Fig 2). At the calibration velocity the water paths are measured by the other two probes meant for actual measurement. (fig.3) Then the ID value measured by mechanical method is subtracted from the summation of two water paths measured by two measurement probes. It gives us the value of probe-to-probe face distance within the inspection head and this value will be constant during all measurements. Probe to probe face distance is not possible to measure by mechanical measurement due to the geometrical layout & probe positions. For measurement of water paths in full wave rectified flank measurement method; the difference between 1st & 2nd interface echoes are measured and in negative half wave rectified peak measurement method the difference between initial pulse and first interface echo is measured. Since the Pressure Tube (PT) is filled with heavy water; during ID measurement inside the coolant channel, there is a need in the inspection head to have a reference calibration probe to measure in-situ calibration velocity. Since the ID value is required with high accuracy, Ultrasonic flaw detector is required to get the water path reading at least with 10 microns reading accuracy as mentioned above.

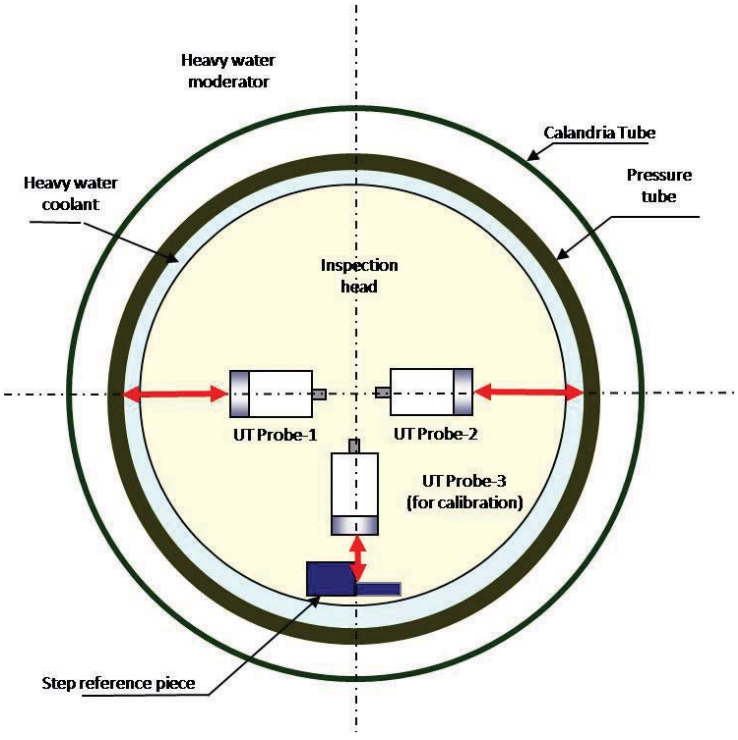

Fig.1: Schematic of Ultrasonic probes arrangement for ID measurement

Fig.2: Echoes from Stepped Reference Block

Fig.3: Water Path Measurement by Ultrasonic Probe

Since actual measurements are done in the channel filled with heavy water, calibration of Inspection heads are also carried out using virgin heavy water before putting into the actual channel. Measurement of Ultrasonic velocity at each measurement location within the channel compensates the Ultrasonic velocity in heavy water at the channel temperature and all measurements within the channel are taken with the measured Ultrasonic velocity in both the techniques.

Measurement Methodology:

$$D = \left(\frac{TOF_1}{2} + \frac{TOF_2}{2}\right) \times v + x \qquad (1)$$

D = Diameter of Pressure Tube, in mm

TOF1 = Ultrasound Time of Flight from probe 1, in μs

TOF2 = Ultrasound Time of Flight from probe 2, in μs

v = Ultrasound velocity in liquid (viz. Heavy water) medium, in mm/μsec

x = Probe to probe face distance for probe 1 & probe 2, in mm

Velocity calibration from stepped piece,

$$v = z/\left(\frac{TOF_{s2}}{2} - \frac{TOF_{s1}}{2}\right) \qquad (2)$$

v = calibration velocity, in mm/μsec

z = step distance from reference piece, in mm.

TOFs1 = Ultrasound Time of Flight from surface 1, in μs

TOFs2 = Ultrasound Time of Flight from surface 2, in μs

Possible errors during ID measurement:

1) Mechanical configuration of the stepped surface such as chamfering, surface roughness, degree of parallelism etc
2) Ultrasonic instrument settings
3) Errors in measurement of probe to probe face distance
4) Variation in light water/heavy water velocities
5) Distance between stepped reference piece used for calibration and reference ultrasonic probe.

Features to achieve the measurement accuracy:

The difference in thickness of two stepped reference block was made to ~18 mm. This will ensure the increased accuracy of water path measurements which is the range of 15-20 mm during actual inspection.

The surfaces of reference block for in-situ velocity measurement has been smoothly polished. In order to achieve sharp stable echoes; the surface

finish of the reference target is made of the order of 0.1 micron or better and two stepped surfaces parallelism is maintained within 10 microns.

The water distance measured by probe is adjusted in such a way that first interface and second interface echoes are having almost equal heights in flank method. This significantly contributes increase in measurement accuracy.

ID measurement in calibration Tube piece is made by two axis coordinate measuring machines where inaccuracy is negligible and minimizes errors in ID values used during calibrations.

Calibration is done before putting the inspection heads into the channel. Inspection heads are calibrated using both light water and heavy water and ID values obtained are compared with mechanical measurement ID data of calibration Tube piece (which is done by two axis coordinate measuring machines). The difference between ID by mechanical measurement and ultrasonic measurement during calibration is always of the order of ± 50 microns.

Considering all other uncertainties in the measurement, the overall accuracy of ID measurement system achieved is approx. ±100 microns.

Calibration Procedure:

First the velocity in the calibration media (first light water, then heavy water) is determined using reference probe with the help of stepped reference block. The reference probe distance from the stepped block is adjusted in such a way that the amplitudes of echoes from the two interfaces of stepped block is almost same (max variation of ± 5% FSH) at any gain (dB) in flank method when put in heavy water during calibration.

Similarly in negative half wave rectified peak method, the distance between initial pulse & 1st interface echo is measured and in this method the echo amplitude can be kept at any height on the screen. Probe to probe face distance is measured in both light water and heavy water during calibration at minimum 3 locations and the difference between these measurements cannot be more than ± 30 microns in both flank and peak method.

The calibration spool of Pressure Tube is around 500mm long. At the centre of the Tube four axial locations (min 50mm apart) are marked as P, Q, R and S. At each axial location, 3 circumferential orientations viz; 6 – 12 O' clock, 4 – 10 O'clock and 2 – 8 O'clock are marked with respect to a fixed reference. All these points are defined as calibration locations and there are 12 such calibration locations in calibration spool.

First the calibration is to be done using light water. At first calibration location, probe to probe distance is determined. This is done by measuring water path at that location using two measurement probes at reference velocity set as mentioned above. The sum of the water path by both measurement probes is to be subtracted from the ID value measured by mechanical method. This probe to probe face distance is a mechanical parameter and remains constant irrespective of media and calibration locations. The measurement of this probe to probe distance is thus repeated at other two locations. The difference of these measurements should not vary by more than ±30μm (microns) as mentioned earlier. The mean of probe to probe face distance measured in heavy water is used during actual ID measurement within the Pressure Tube in both the methods.

After that in remaining 9 calibration locations, using average probe to probe face distance determined above, ID values by Ultrasonic method

are calculated and they are compared with mechanical ID measurement values. The difference of ID determined by UT method and mechanical method does not vary by more than ±50μm for any calibration locations.

The distance between the measurement probes and the ID of the tube is adjusted in such a way that the amplitudes of the first and second interface echoes shall be almost same (max variations ± 5% FSH at any gain level) in flank method. In velocity measurement interface echoes from two steps shall be kept within the width of 'A' and 'B' gates respectively and difference in the beam path between the gates measured in flank/edge mode. In water path measurement, 1st and 2nd interface echoes are kept within gates A and B respectively (gate threshold level to be kept at 40 % FSH for both the gates) and their differences are measured in flank/edge mode. Measurement of Velocity of Ultrasound in Light Water was carried out using negative half-wave rectification on the echo signals received from two steps of the reference block. Two Gates used one each on the two echo signals from the step reference block. Measurement of reference velocity using Peak method of water path measurement, by entering the precise step difference measured mechanically. Then the distance between initial pulse & 1st interface echo is measured and in this method the echo amplitude can be kept at any height on the screen.

Measurement of Probe Face-to-Face distance was carried out in the Calibration tube by measurement of water paths of Probe-1 and Probe-2 and subtracting sum of the two water paths of Probe-1 and Probe-2 from the Calibration tube ID. Water path measurement of Probe-1 and Probe-2 at each location was carried out using Peak Measurement mode with one gate on the First Interface (S-A mode in the UT equipment) of the negative half-wave rectification echo signal received from ID of the tube.

Measurement of Internal Diameter was carried out in horizontal condition in both 3-9 O'clock and 6-12 O' Clock orientation in the Test Set Up for 2%, 4% and 5% diametrical creep tube samples by both the methods. The ID at each location was calculated by summation of Water paths of Probe -1, Probe-2 and Probe Face to Face distance.

During calibration, the temperature of the water should be measured. Similar exercise of calibration is repeated (in exactly the same manner as in light water) using virgin heavy water in a calibration tank and data are to be tabulated in a similar format. The accuracy level required for probe to probe face distance measurements and ID measurements at 9 other locations shall be same as of light water calibration.

For validation of technique for higher diameter pressure tubes in the actual coolant channel, experiments were also carried out using 2%, 4% & 5% creep ID standards and accuracy of ID measurements were found to be approx. ±100 microns as described in Para 7.0(Results & discussions). All calibrations are to be done using full length signal cable and four drive tube cables, which simulate the actual condition during inspection. All the parameters of equipment controls are to be recorded and used during actual inspection for setting of Ultrasonic equipment.

RESULTS AND DISCUSSION:

This ID measurement technique has been successfully used in various Pressurized Heavy Water reactors (PHWRs). This has also been deployed in both types of Indian PHWRs viz. 220 MWe & 540 MWe. Measurements were generally done at 3-9 O'clock orientation and also at 6-12 O'clock orientation in a cross section with a close spacing (100 mm) between two successive measurements for ID in the hot region (where diameter increase is expected to be higher) to find out the maximum

Flank Mode ID Measurement

Sr. No.	Inspection Head Type and No.	Diametrical Creep (Tube Sample Size)	Maximum variation between UT ID and Mechanical ID (in mm)
1	220 MWe NDG-12-10	2%(84.15mm)	+0.03 /-0.03
2		4%(85.80mm)	+0.07/-0.03
3		5%(86.60mm)	+0.08/-0.13
4	540 MWe BDG-12-06	2%(105.50mm)	+0.01/-0.08
5		4%(107.60mm)	+0.10/-0.07
6		5%(108.60mm)	+0.11/-0.01

Peak Mode ID Measurement

Sr. No	Inspection Head Type and No.	Diametrical Creep (Tube Sample Size)	Maximum variation between UT ID and Mechanical ID (in mm)
1	220 MWe NDG-12-10	2%(84.15mm)	-0.03 /-0.05
2		4%(85.80mm)	+0.04/-0.01
3		5%(86.60mm)	+0.05/-0.04
4	540 MWe BDG-12-06	2%(105.50mm)	-0.04/-0.07
5		4%(107.60mm)	+0.08/+0.01
6		5%(108.60mm)	+0.09/-0.11

diameter in the channel. At other than the hot region, axial spacing between two successive locations is 200 mm. The difference in ID values at 6-12 O'clock and 3-9 O'clock orientations at same axial location was also observed and found to be very less as can be seen from the graph (Fig -4) given below. This ensures that de-centering errors of Inspection head in the channel was also negligible. This was also successfully carried out for 540 MWe PHWRs at TAPS 3&4 .Apart from that at rolled joint region & liner tube region where possibility of increase in diameter is very less, ISI values are almost matching with installed data within max. difference of ±50μm (microns). This ensures the required accuracy obtained from our ID measurement technique.

The two techniques (Flank and Peak) were simultaneously employed in K-04 channel of KGS-1 and the data obtained by both the methods were compared and plotted as graph (fig 5 & 6). The RF waveforms for both types of UT signals were captured and analyzed (fig 7). It has been observed from RF waveform analysis that negative half wave rectified peak method gives better accuracy than full wave rectified flank method.

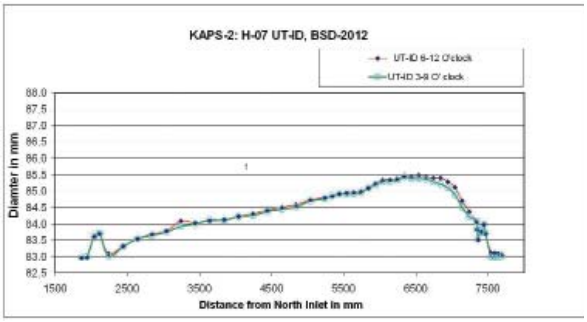

Fig. 4: UT-ID for Channel H-07 KAPS-2

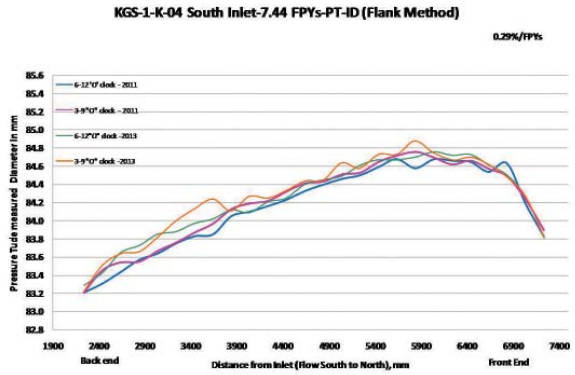

Fig. 5: UT-ID for Channel K-4 KGS-1 (Flank Method)

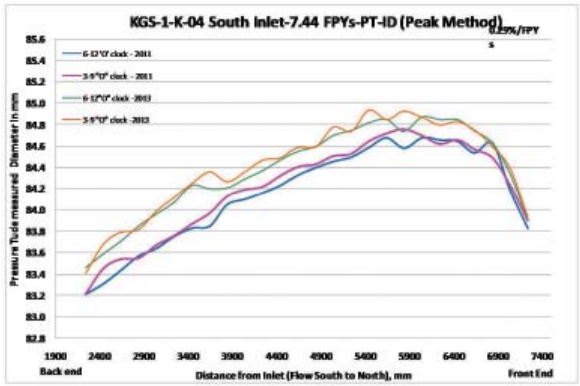

Fig. 6: UT-ID for Channel K-4 KGS-1 (Peak Method)

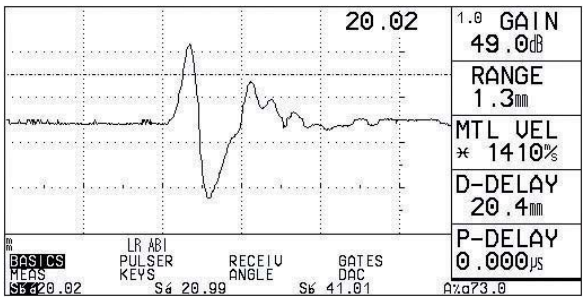

Fig. 7: RF Waveform

CONCLUSION:

ID measurement using our above mentioned techniques for all PHWR's (both 220 MWe and 540 MWe) was carried out successfully. From our experiences it is observed that ID measurement of Pressure Tube in in-situ condition is possible with this probe arrangement and digital Ultrasonic flaw detector. We also make the provision of in-situ calibration with the help of calibration probe and stepped reference reflector at fixed distance for compensation of Ultrasonic velocity in heavy water at the channel temperature. The inspection head has been designed in such a way that it can measure the ID of Pressure tube at any circumferential and axial locations for monitoring the growth of diameter due to high temperature irradiation and creep with required accuracy. It also helps in determining ovality of Pressure Tube. The results obtained from different reactors are highly encouraging and presently it is regularly used during Pre-Service & In-Service inspection of any 220 MWe & 540 MWe PHWRs.

ACKNOWLEDGEMENTS:

The authors deeply acknowledge the guidance, support and encouragement from Shri R.J.Patel, Head, RTD, BARC & Chairman of the sub-committee for evaluation of PT UT ID measurement technique formed by Expert Group of Coolant Channel and also from the other members of that subcommittee for their timely help & prompt action for evaluation of experimental data.

REFERENCES:

1. IAEA-TECDOC- 1037; Assessment and management of aging of major Nuclear Power Plant Components: Important to safety
2. CAN/CSA-N285.4-94; Periodic Inspection of CANDU Nuclear Power Plant Components.
3. AERB Safety Guide: AERB/NPP/SG/O-2

National Symposium on Very High Energy Gamma – Ray Astronomy (NSGRA-2013): a report

The National Symposium on Very High Energy Gamma-Ray Astronomy was organized jointly by the Astrophysical Sciences Division, BARC and the Department of High Energy Physics, TIFR during 25-27 November, 2013 at the Training School Hostel, BARC, Mumbai. About 90 delegates from various national institutes and universities participated. 12 invited talks on various aspects of multi-wavelength observations were organized during the morning sessions and 30 contributed papers were presented in the afternoon sessions. 10 posters on various aspects of ground-based gamma-ray astronomy were also displayed. On the last day special sessions were organized to discuss the status of the MACE and HAGAR gamma-ray telescopes. A panel discussion was also organized to discuss the need for Indian participation in the Cherenkov Telescope Array (CTA) project – a VHE observatory being set up by an international collaboration of 170 institutes from 27 countries. Prof. S. Ananthakrishnan, Pune University, Prof. P. Sreekumar, Director, IIA, Bengaluru, Prof. V.C. Sahni, BARC, Prof. P.R. Vishwanath, Ex TIFR, Prof. B.S.Acharya, TIFR, Dr. V. Chitnis, TIFR, Shri. Y.S. Mayya, BARC, Shri R. Koul, BARC, Dr. R.C. Rannot, BARC, Dr. A.K. Mitra, BARC, Dr. A.K. Tickoo, BARC and many other delegates participated in the discussions. It was the considered opinion of the delegates that participation in the CTA project would be beneficial to the astronomy and astrophysics community of the country. It was suggested that the details of possible in-kind contribution to the CTA be worked out and a project report be submitted to DAE for funding. The symposium was funded by BRNS and TIFR.

A group photograph of the participants of the NSGRA-2013

Report of Conference on Neutron Scattering (CNS-2014)

A Conference on Neutron Scattering was held at the Indian Institute of Science and Education Research (IISER), Pune, during February 10 - 12, 2014. It was sponsored by the Board of Research in Nuclear Sciences. The conference was jointly organized by BARC and IISER Pune in association with the Neutron Scattering Society of India (NSSI). The conference was inaugurated by Prof. S.L. Chaplot, Director, Physics Group, BARC. Prof. H. Schober, Associate Director - Science Division, Institut Laue-Langevin, France, was the Chief Guest at the inaugural function. Prof. K.N. Ganesh, Director, IISER, Pune and Prof. R. Mukhopadhyay, Head, Solid State Physics Division, BARC also addressed the audience during the inaugural function.

There were more than 125 participants including 9 invited speakers from abroad. There were 31 invited talks and about 100 poster presentations. The conference covered important aspects of neutron scattering including facilities, science and applications. Particular emphasis was given to the application of neutron scattering in strongly correlated electron systems, functional materials, soft matter and biological systems, thin films and multilayers, and nanomaterials.

Researchers from various universities and national institutions regularly utilize the National Facility for Neutron Beam Research at Dhruva reactor, BARC. The conference provided useful scientific discussions and a platform for collaborations among the national and international neutron scattering researchers. Four best posters were awarded by the NSSI.

A Pre-Conference Neutron School on "Neutron as Probes of Condensed Matter" (XVI in the series) was organized prior to CNS-2014 jointly by BARC and UGC-DAE-CSR during February 4 - 8, 2014. The course comprised theory lectures and hands-on experiments at Dhruva reactor. Apart from the faculty of BARC and UGC-DAE CSR, some of the foreign invited speakers to the conference delivered lectures in the School.

A group photograph of participants of CNS-2014 at IISER, Pune.

Report on National Symposium on Nuclear Instrumentation – 2013 (NSNI-2013)

The National Symposium on Nuclear Instrumentation (NSNI-2013) was held at the Multi-purpose Hall, Training School Hostel, AnushaktiNagar, Mumbai during November 19-21, 2013. The Conference was organized by Electronics & Instrumentation Group, BARC under the aegis of BRNS. The DAE-BRNS symposium covered application areas of Nuclear Instrumentation for Reactors, Accelerators, Physics Experiments, Health and Environment Monitoring Systems. Topics covered in the symposium included radiation detectors, front-end electronics, RF electronics, Smart instruments, High density / high performance systems, Instrumentation bus and communication standards and Software technologies.

This symposium was organized to provide a forum for scientists and engineers to present their work and share their knowledge and ideas with other participants in the field. The Conference was attended by more than 300 participants from AMD, BARC, IGCAR, IUAC, IPR-ITER, NPCIL, RRCAT, TIFR, UCIL, VECC and HBNI as well as from academic institutions.

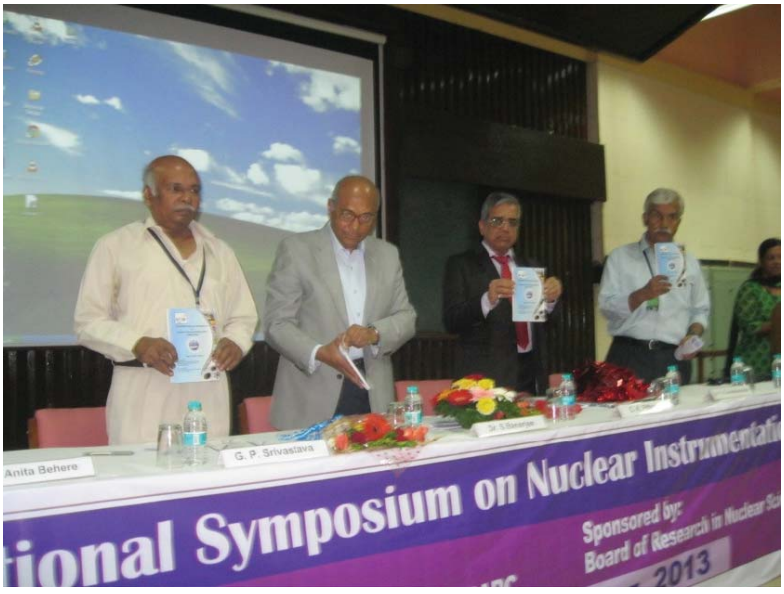

Photograph of the proceedings of NSNI-2013 being released by Dr. Srikumar Banerjee, the Chief Guest

Dr. Srikumar Banerjee, Prof. Homi Bhabha Chair and Former Secretary, DAE & Chairman AEC presided over the inaugural function. Dr. T.S. Ananthakrishnan Head, Electronics Division and Chairman, Organizing Committee welcomed the invitees and delegates of NSNI-2013. Shri C.K. Pithawa Director E&I Group and Chairman National Advisory Committee presented an overview of NSNI-2013. Shri G.P. Srivastava, OSD and Former Director E&I Group delivered the keynote address. Chief Guest Dr. S. Banerjee delivered the inaugural address and formally released the Symposium Proceedings. Anita Behere Convener, Organizing Committee proposed the vote of thanks.

Contributions were received in the form of 128 poster papers which were presented in five sessions. The posters for all the contributory papers were prepared by the authors in a uniform template provided by organizers and were printed by the organizers. They were put on display and were presented by the authors. There was a collective preview presentation for each poster session where each poster was introduced to the audience through a summary slide that illustrated the paper.

The main highlight of the symposium was the invited talks (21) on topics related to application areas of Nuclear Instrumentation. Speakers from BARC, IGCAR, NPCIL, RRCAT, IIT (B) and IIT Roorkee were invited to deliver the talks. Notable speakers from abroad include Dr. Shekhar Mishra, from Fermi Labs and Dr. Andrea Venturi from CERN. Proceedings of the symposium were brought out in the form of CDs.

Resistive Plate Chambers installed for the new layer added to CMS muon system at CERN

A fourth station — called RE4 (Resistive Plate Chambers for the Fourth End-Cap)— will be added to the CMS endcap muon system during the ongoing LHC Long Shutdown (LS1 – 2013-2014). The CMS muon system consists of three different sub-detectors: RPCs (Resistive Plate Chambers), DT (Drift Tubes)and CSC (Cathode Strip Chambers). The endcap region is made of CSCs and RPCs in the first three disks and RPCs will be installed in the fourth disk as part of the RE4 project. The construction of the RE4 is an international project carried out by teams from institutes in Belgium, Bulgaria, China, Colombia, Finland, Georgia, India, Italy, Korea, Mexico and Pakistan as well as from CERN.

CERN plays an important role in the chamber construction and testing at the RPC laboratory located in building 904 at Prevessin where many physicists, engineers, technicians and students from around the world are working together, alongwith the assembly sites in Belgium (University of Ghent) and India (NPD-BARC). RE4 consists of 72 super-modules, each of which is made by two RPCs (Fig. 1), for a total of 144 double-gap RPCs. Nineteen institutions involved with the RPCs cover all the tasks and have been working very hard since the beginning of 2012, in order to complete the project by the end of 2014. These tasks are distributed among the following countries: Korea is responsible for the construction of 660 gas gaps and 10 chambers. Pakistan, Italy and Finland are working on the front-end electronics, DAQ and power system while India (NPD-BARC) is building and characterizing 50 RPCs, apart from fabricating 200 cooling sets (MD&PDD-BARC) for the entire collaboration. Bulgaria, Mexico and Georgia are responsible for super-module assembly and testing. India, Italy and Pakistan are building

Fig. 1 : The Super Module Assembly

Fig. 2 : The recently installed, positive side of the RE4, 100 metres below the ground, at Point 5 (CMS at the LHC facility) in Cessy, France is approximately 15 metres in diameter, weighing close to 5 tons

the chamber services (gas, cooling and cabling). China provides the readout strips, mechanical frame boxes and participates in the chamber construction and testing at CERN. A large international team will work on the installation and commissioning of the full system. So far, the three assembly sites have produced 72 RPC detectors, corresponding to 36 super-modules; these were installed earlier in December 2013 (Fig. 2 – positive side of endcap). The production for the second endcap disk (negative side) started in September 2013 and is almost getting completed. The installation and commissioning of the same is scheduled during middle of 2014.

The Nineteenth National Symposium & Workshop on Thermal Analysis (THERMANS-2013)

The Nineteenth National Symposium & Workshop on Thermal Analysis (THERMANS-2013) was held at TSH & HBNI, BARC during December 19-23, 2013.

There was overwhelming response to the symposium and workshop. In all there were 240 registered participants from academic and research institutions with a significant percentage of students and research scholar participants.

The symposium was inaugurated by Dr. K.L. Ramakumar Director, Radiochemistry & Isotope Group, BARC. Dr. B.N. Jagatap, Director Chemistry Group was Guest of Honour for the inaugural function. Dr D. Das, President, Indian Thermal Analysis Society (ITAS) cited the active role played by thermal analysis techniques in characterization of materials for specific purposes.

Dr. S.C. Parida, Secretary, ITAS, announced the awards instituted by the Indian Thermal Analysis Society. The awards were presented by Dr. K.L. Ramakumar, Dr. B.N. Jagatap, Dr. D. Das and the sponsors of the awards. SETARAM-ITAS Calorimetry Excellence Award was conferred on Dr. V. Venugopal. NETZSCH-ITAS Award 2013 for her outstanding contributions to field of thermal analysis was conferred on Dr. (Mrs.) Bina N. Wani, of Chemistry Division BARC, Mumbai. The TA Instruments-ITAS Young Scientist Award 2013was conferred on Shri Bhaskar Paul of Materials Processing Division, BARC. Dr. M.D. Karkhanavala Memorial Essay Contest 2013 was won by Shri Subhasis Pati, JRF, BARC. Dr. Gurdip Singh Award for Best Thesis in Thermal Analysis 2013 was given to Dr. Puja Paul of Jadavpur University, Kolkata.

There were 08 technical sessions, 01 instrumentation session and 13 invited lectures. More than 120 research papers were presented at the symposium in both oral and poster sessions.

Inaugural function of THERMANS 2013. From right to left: Dr. K.L. Ramakumar (Director, Radiochemistry and Isotope Group, BARC), Dr. Shyamala Bharadwaj (Convener, THERMANS 2013), Dr. B.N. Jagatap (Director, Chemistry Group, BARC), Dr. D. Das (President, ITAS) and Dr. Y. K. Bhardwaj (Secretary, THERMANS 2013)

BARC Scientists Honoured

Name of the Scientist	:	Pitamber Singh, IADD
Name of the Award	:	Fellowship Award under Physics category
Instituted by	:	International Academy of Physical Sciences(IAPS)
Name of the Event	:	Academy conference on "Science and Technology for sustainable development" held at Indian Institute for Information Technology, Design and Manufacturing (IIITDM) Jabalpur, 20th March, 2014

Name of the Scientists	:	Pramod Bhatt and S.M. Yusuf, SSPD
Name of Award	:	Best Poster Award
Title of the Paper	:	Neutron diffraction and reverse Monte Carlo simulation study of M1.5[Cr(CN)6]•zH2O (M= Fe,Co,Ni) Prussian blue analogues molecular magnets
Presented at	:	7th India-Singapore Symposium on Experimental Condensed Matter Physics (2014) held at Mumbai, 24-26 February 2014.

Name of the Scientist	:	A.K. Tyagi, Chemistry Division
Name of the Award	:	MRSI-ICSC Superconductivity and Materials Science Senior Award (2014)
Instituted by	:	Materials Research Society of India at the Conference held at Bengaluru, Feb. 12-14, 2014

Name of the Scientist	:	K. Dasgupta, REDS, Materials Group
Name of the Award	:	Best Presentation Award
Title of the Paper	:	Development of rare-earth based magnetic alloy powders by reduction-diffusion method
Presented At	:	International Conference on Magnetic Materials and Applications (MagMa 2013), Guwahati, Dec.5-7, 2013.

Name of the Scientists	:	Sangeeta Deokattey, K. Bhanumurthy and P.K. Wattal
Affiliation	:	SIRD and NRG
Title of the Award	:	Progress in Nuclear Energy Best Paper Award 2013
Instituted by	:	The Editors of the Journal
Title of the Paper	:	High Level Waste Management in Asia : R&D Perspectives, Vol. 62, Jan 2013, pp. 37-45.

Cirus & Dhruva Research Reactors at BARC

Edited & Published by:
Scientific Information Resource Division
Bhabha Atomic Research Centre, Trombay, Mumbai 400 085, India
BARC Newsletter is also available at URL:http:www.barc.gov.in